

Computational Modeling of the Phase Diagram of Magnetic Skyrmions

Yifan Zhou

MSc by Research

University of York

Physics

December 2016

Abstract

Magnetic skyrmions are vortex-like spin structures that appear in magnetic materials with Dzyaloshinskii-Moriya(DM) interactions and exchange interactions. Their small size and inherent stability suggest the potential application in magnetic memory systems. A well-defined phase diagram of skyrmions is important for investigating their stability. This is a complicated task due to the topological nature of magnetic skyrmions, whose phase transitions are not obviously illustrated by general parameters such as total energy and magnetization. In this thesis, we have developed a methodology in determining the phase diagram of the skyrmion lattice model by performing the atomistic spin simulation. We investigate the spin states of the lattice in the magnetic fields at zero temperature first, then apply finite temperatures in studying the phase transition between the skyrmion state and other states. At 0 K we find five spin states in varying magnetic fields. In the skyrmion state, the ratio between DM interaction and exchange interaction, together with the magnetic anisotropy affect the size and shape of skyrmions. At finite temperatures, the thermal stability of the skyrmion lattice is shown by a contour plot of the skyrmion number as a function of external field and temperature. The loss of lattice symmetry with a growing temperature is demonstrated by the spin configurations of the lattice in the real and reciprocal space. We then characterize the phase transition of the skyrmion state by several specific parameters, such as the specific heat capacity, the static magnetic susceptibility and the skyrmion life time. The parameters show similar critical temperature of the skyrmion state. Specifically, the skyrmion life time of the applied model follows the Arrhenius law as a function of temperature. We also discuss the effect of the femtosecond heat and magnetic pulse on the nucleation of the skyrmion state.

Contents

Abstract	2
Contents	3
List of Figures	6
Acknowledgments	11
Declaration	12
1 Introduction	14
2 Theoretical Background	18
2.1 Atomistic spin model of magnetism	18
2.1.1 Classical spin Hamiltonian	18
2.1.2 General matrix expression of interaction	19
2.1.3 Exchange interaction	19
2.1.4 Magnetic anisotropy	20
2.1.5 Applied field	21
2.1.6 Dzyaloshinskii-Moriya interaction	21
2.2 Atomistic spin dynamics	22
2.2.1 Landau-Lifshitz-Gilbert equation	22
2.2.2 Langevin dynamics	23
2.2.3 Time integration	24
2.3 Monte Carlo method	26
2.4 Magnetic skyrmions	27
2.4.1 Definition of skyrmions	27

2.4.2	Physical origins of magnetic skyrmions	28
2.4.3	Summary	29
3	Existence Criteria for the Skyrmion Phase at 0 K	30
3.1	Example of skyrmion lattice	30
3.2	Constant material parameters	32
3.2.1	Spin states with varied magnetic field	33
3.2.2	Spin states without magnetic field	36
3.3	Varied material parameters	39
3.3.1	DM interaction and exchange interaction	40
3.3.2	Magnetic anisotropy	42
3.4	Summary	43
4	Thermal Phase Diagram of the Skyrmion Lattice	44
4.1	Equilibrium phase diagram	45
4.1.1	Topological energy barrier	46
4.2	Analysis of spin figures	48
4.2.1	Spin figures in real and momentum space	49
4.2.2	Skyrmion deformation and interaction	50
4.3	Parameters for the phase diagram	51
4.3.1	Specific heat capacity	52
4.3.2	Static Magnetic Susceptibility	52
4.4	Skyrmion life time	53
4.4.1	Simple model of the skyrmion time decay	54
4.4.2	Calculation of the life time	55
4.4.3	The Arrhenius Law	57
4.5	Creation of the skyrmion state by femtosecond pulse	59
4.5.1	Effect of femtosecond heat pulse	59
4.5.2	Additional magnetic pulse	61
4.6	Summary	62
5	Conclusion	63
5.0.1	Future outlook	64

CONTENTS

Appendix A	The skyrmion number on a discrete lattice	66
Bibliography		68

List of Figures

1.1	Typical topological structures of the magnetic skyrmions: a, a Bloch-type skyrmion; b, Neel-type skyrmion. Extract from [1]	15
2.1	Simplified form of two dimensional DM interaction within neighboring atoms: atom 1 (orange circle) is interacting with four atoms (blue circles), of which directions are indicated by feint black arrows. Detailed equation of DM interactions between spin 1 & 2, 1 & 3 are given.	22
2.2	The analytical solution is plotted in the lines, comparing with the points for computational approach. Panel (b) and (d) illustrate the error traces for two damping constants for (a) and (c). The error is in the magnitudes of 10^{-6} , which shows good correspondence. Extract from [2].	26
3.1	The thermal field-cooling in red line starts from 20K, cooling to 0K in 2ns. The constant magnetic field of 3.2 T is shown as the blue line.	31
3.2	The spins are represented by colored arrows, where the color scale linearly depends on their value in z -component, with blue for -1 and red for +1. The skyrmion structure is clearly shown in the whole lattice with an hexagonal structure.	32
3.3	The total energy, skyrmion number and magnetization of each spin states, divided as a-e in the figure.	34
3.4	(a)-(e): five spin states under varied range of perpendicular magnetic field. Top-right part in each figure is the spin state in the momentum space.	34

LIST OF FIGURES

- 3.5 The thermal field-cooling in red line still starts from 20 K, cooling to 0K in 2 ns. The constant magnetic field is cutoff once field-cooling finished, as the blue line in 3.0 T. 37
- 3.6 The comparison shows roughly the same skyrmion number with and without magnetic field, indicating the topological stability of the skyrmions. The total energy become higher in skyrmion states without magnetic field, while ferromagnetic state without the magnetic field is extremely unstable. 37
- 3.7 In the **b: Spiral-Skyrmion State**, some of the skyrmions still survive, while some vanish to form part of a stripe. 38
- 3.8 In the **c: Skyrmion State**, the skyrmions collectively enlarge without the magnetic field. 38
- 3.9 In the **d: Skyrmion-Ferromagnetic State**, the spin configure become a mixture of mainly stripes with a randomly distributed skyrmion. 38
- 3.10 The DM interaction D is fixed to be 1 meV, and the exchange interaction J ranges from 1 meV to 5 meV. The magnetic field B shown above is calculated from (3.3) with $c = 0.2$. The solid line on the spin figures demonstrates the pitch length of the skyrmion diameter. 40
- 3.11 The exchange interaction J is fixed to be 1 meV, and the DM interaction D ranges from 1 meV to 5 meV. The magnetic field B is calculated from (3.3) with $c = 0.2$. The solid line on the spin figures demonstrates the pitch length of the skyrmion diameter. 41
- 3.12 The theoretical size curve (red line) 3.4 and the counted size (blue point) are plotted together. p is the pitch length of the skyrmion diameter. The two values show a good accordance. 41

3.13 The contour plot consists by the skyrmion number as a function of the anisotropy and the magnetic field. The solid line indicates the skyrmion number of 6, which is nearly the half of the maximum number. Spin figures of three vertices of this triangle-like range are chosen to illustrate the magnetic configurations in the next figure, as shown by black dots in the plot: 1.(-1,1); 2.(1,1); 3.(1,9.5). 42

3.14 (1): with 1 meV easy axis anisotropy and 1 T perpendicular magnetic field, the skyrmions shrink significantly and disperse on the lattice, similar to the skyrmion-ferromagnetic state. (2): with 1 meV easy plane anisotropy and 1 T perpendicular magnetic field, the skyrmions enlarge in the shape of square. (3): with 1 meV easy plane anisotropy and 9.5 T perpendicular magnetic field, the ordered skyrmions still exist on lattice in large field. 43

4.1 The total energy and magnetization with temperature: each point is calculated as the average value over several nanoseconds in thermal equilibrium. The two parameters change continuously with increasing temperature. 45

4.2 The contour diagram is consisted by the skyrmion number over temperature and perpendicular magnetic field. The color bar on the right side shows the magnitude of the skyrmion number. The solid line indicates a skyrmion number of 6, which is half of the maximum skyrmion number of the lattice. 46

4.3 The skyrmion number of the skyrmion lattice without magnetic field: the skyrmion number here is calculated at thermal equilibrium at each temperature. The skyrmion structure stabilizes below 0.8 K, and experiences a transitional phase in range of 0.9 K to 1.3 K. The topological structure is totally broken at 1.4 K and above. 48

LIST OF FIGURES

4.4	The real-space spin figures and Fourier intensity at 1-8 K. The central peak ($k = 0$) is the largest value in the momentum space. The Fourier points are scaled with gray level, i.e white as zero and black represents the largest value. Left column from top: T= 1 K, 2 K, 3 K and 4 K; right column from top: T= 5 K, 6 K, 7 K and 8 K.	49
4.5	At 4 K, 6 K and 8K, two spin figures are chosen, with 1 ns time interval.	51
4.6	The specific heat capacity in the skyrmion state. In this state, the heat capacity shows a peak at around 6 K.	52
4.7	The static magnetic susceptibility in the skyrmion state. In this state, the susceptibility shows a phase change at around 6 K. . .	53
4.8	The process starts with the field cooling by 2 ns, followed by 3 ns equilibrium time in 0 K. A constant temperature of 6 K is applied at 5 ns. A constant perpendicular magnetic field of 3.2 T exists in the whole procedure.	54
4.9	(1)-(12): the fitting of real-time data of the skyrmion number with time to (4.6) at different temperatures from 1 K to 12 K. the red line is the real skyrmion number calculated from the lattice at each time step of 5 ps, and the blue line is the fitting curve by (4.6). The number indicated showing the fitting life time of the skyrmions at each temperature in the unit of 5×10^{-12} s.	56
4.10	The logarithm skyrmion life time in each temperature with the error bar from the fitting in figure 4.9. The temperatures from left to right decrease from 12 K to 5 K, thus the reciprocal $1/T$ increases. The logarithm life time is fitted linearly from 12 K to 6 K, while gradually deviates from the fitting curve from 6 K to 5 K, indicating a transition from purely diffusive behavior to a topologically protected state.	58
4.11	The origin spiral state for the simulations in this section.	59

LIST OF FIGURES

4.12	The conditions and the consequent spin figures for the heat pulse: the left column is the conditions of each simulation, and the right column shows the spin figures under each condition.	60
4.13	The conditions and the consequent spin figures for the heat pulse and the magnetic pulse: the left column is the conditions of each simulation, and the right column shows the spin figures under each condition.	61

Acknowledgments

I would like to express my gratitude firstly to Professor Roy Chantrell for giving me the opportunity to study and work in this excellent research group. He helped me a lot with his patience and encouraged me with his enthusiasm during those hard times. It has been a privilege to perform my Master under his guidance. I am also grateful to the Dr. Richard Evans for offering me an excellent computational tool, the VAMPIRE, to discover the fascinating world of magnetism. He has given me many useful advice on the simulation.

I would like to thank Sergiu Ruta and Andrea Meo for their countless supports, cooperation and of course friendship. I indeed enjoyed to talk with them, which inspired me deeply during my research. I also would like to thank my colleagues in the group for providing a good atmosphere and useful suggestions, Dr David Serantes, Samuel Westmoreland, Razvan Ababei, Dr Chudong Xu.

Last but not the least, I would like to thank my family and my friends for their sincere supports. They inspired my will throughout my Master study and my life in general.

Declaration

I declare that this thesis is a presentation of original work and I am the sole author. This work has not previously been presented for an award at this, or any other, University. All sources are acknowledged as References.

I would like to dedicate this thesis to my beloved grandmother.

Chapter 1

Introduction

The concept of Skyrmion originates from nuclear physics, initially proposed by Tony Skyrme to describe mesons and baryons in nonlinear field theory[3]. The mathematical definition of the skyrmion is now applied widely in condensed matter physics, such as liquid crystal[4], Bose-Einstein condensation[5], and especially in the area of magnetic materials[6]. The magnetic skyrmions exhibit two types of topological spin structures: the Bloch type, which the spins rotate in a plane perpendicular to radial directions from the center to the periphery, and the Neel type, which the spins rotate along the radial directions, as is shown in figure 1.1. Several theoretical predictions of the skyrmion structure were proposed as one of the thermodynamically stable spin vortex states in magnetic materials[7][8][9]. It was not until 2009, two decades after the initial theoretical work, that the existence of such a spin structure was validated by a set of experiments[10][11][12]. Skyrmions in ultra-thin film, which is the focus of this thesis, was observed later experimentally by the spin polarized scanning tunneling microscope (STM) of Fe on Ir(111)[13]. There are several attractive characteristics that suggests the potential application of the skyrmion spin structure: firstly, the size of the skyrmions can be reduced to a few nanometers, leading to a higher density of the magnetic information storage. Secondly, the skyrmions are topological solitons that cannot be bent into a uniform state, which improves their stability against both external changes and inner defects. Thirdly, the skyrmions can be displaced by the spin torque with very low current density, thus saving energy of the information storage[14].

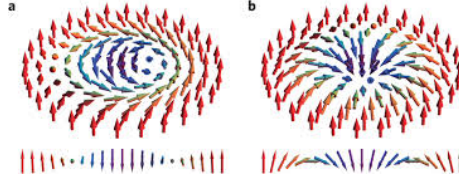


Figure 1.1: Typical topological structures of the magnetic skyrmions: a, a Bloch-type skyrmion; b, Neel-type skyrmion. Extract from [1]

Although there are several mechanisms which give rise to the skyrmion structure[15], the breaking of the inversion symmetry at the interface, known as the Dzyaloshinskii–Moriya interaction (DMI), is the mostly investigated mechanism so far. Such lack of symmetry is mainly induced by the association between magnetic thin films and metals with strong spin-orbit (SO) coupling[16], such as Pt, Ir, W, etc. The advantage of this type of skyrmion is the possibility to tune the DMI by modifying the metal compounds or the number of the layers, thus adjusting the size of the skyrmion and improving their stability as well. It is recently reported that the interfacial DMI-based skyrmions can be observed at room temperature[17], which promises the real-world application of the skyrmion racetrack memory[18].

The numerical simulation of the skyrmions is also intensively investigated as a good complement to the experimental research. The simulations of the skyrmion system include the stabilization, nucleation and propagation of the individual and lattice skyrmions. Numerically, skyrmions are found to be stable for a large range of DMI and exchange interaction[19], and can be nucleated and moved by spin injection through spin transfer torques[20]. However, due to the topological nature of the skyrmion state, it requires unconventional parameters to achieve a well-defined phase diagram. From the previous studies, there are several existing methods and parameters defining the skyrmion phase, while lacking a bottom-up analysis of the whole phase diagram.

The proposal of this work is to give a clear phase diagram of the skyrmion state with the DMI-type lattice model, with the perpendicular magnetic field and with temperature included as a thermal field using Langevin dynamics. In particular, the research combines the spin configurations of the magnetic

structures with the theoretical and phenomenological parameters, leading to a more complete and insightful description of the skyrmion state.

The second chapter gives an overview of the general principles of the physics of magnetism which facilitates further computational study of the magnetic material. It presents the atomistic spin model of magnetism with a detailed discussion of the spin Hamiltonian of the lattice with DMI. Further consideration is given to the numerical methods of calculating the spin dynamics, including the Landau-Lifshitz-Gilbert equation with Langevin dynamics and the Monte Carlo method. The chapter ends with a discussion of the topological and structural properties of magnetic skyrmions, with a summary of some important properties of skyrmions.

In the third chapter, the magnetic skyrmions on the DMI type of lattice at 0 K with perpendicular magnetic field are investigated. An example of typical conditions to nucleate skyrmion state is given, with three major factors included: the exchange interaction, the DMI and the perpendicular magnetic field. In varying magnetic fields, the lattice forms different spin states, among which the skyrmion state covers a wide range of magnetic field. In particular, the spin states after removal of the magnetic field are calculated, showing that the skyrmion lattice survives in zero field, as is experimentally illustrated[21]. In the second part of the chapter, the material parameters are systematically modified. The size of the skyrmions is quantified in terms of the DMI and the exchange interaction. The effect of magnetic anisotropy, on the other hand, is qualitatively discussed.

The fourth chapter consists of a detailed investigation of the skyrmion state at finite temperatures. In the first part of this chapter, a general equilibrium phase diagram of the skyrmion over temperature and the perpendicular magnetic field is given, combined with an estimation of the topological energy barrier of the skyrmions. The spin figures in real and reciprocal space are then introduced, showing that the skyrmions undergo two different developments with the growing temperature: the profile of the skyrmions is changed and the hexagonal structure remains at low temperature, while the hexagonal structure becomes distorted and disappears at high temperature. It is thus important to

quantify the phase diagram to define the region of the ordered skyrmion phase. Inspired by the experiments, additional parameters are applied to study the phase change, namely the static heat capacity and the specific magnetic susceptibility. In addition, the skyrmion life time is a well-defined parameter that describes the thermal annihilation of the skyrmion lattice as an exponential decay, or so-called Arrhenius law. The energy barrier of the skyrmion lattice leads to an exponential relationship between the skyrmion life time and the temperature. This chapter finishes up with a preliminary study on the femtosecond creation of the skyrmion state. Finally, chapter five summarizes the conclusion of the thesis and provides a future outlook.

Chapter 2

Theoretical Background

The research is comprised of computer simulations and theoretical analysis of the magnetic DMI(Dzyaloshinskii-Moriya Interaction) type skyrmion systems. The main program in use is the VAMPIRE[22], which is based on the atomistic spin model of magnetism.

2.1 Atomistic spin model of magnetism

The basic property of the atomistic spin model is to localize unpaired electrons to atomic sites, where each electron is assumed to possess a constant magnetization length. The direction of an atomic magnetic moment is described by a unit vector \mathbf{S}_j [22], which is defined as $\boldsymbol{\mu}_s/|\boldsymbol{\mu}_s|$, where $\boldsymbol{\mu}_s$ is the spin magnetic moment. The Heisenberg model of exchange is applied, and all the possible interactions between neighboring electron spins are considered as well.

In this section, the classical spin Hamiltonian will be introduced first, followed by general matrix expression of interaction and detailed description of main energy contributions.

2.1.1 Classical spin Hamiltonian

The energy of a group of spins is determined both by interactions with each other and with external conditions. As the main part of the total energy, the interactions among the spins originate from overlapping of wavefunction between neighbouring atoms, known as the exchange interaction. Several ex-

2.1. ATOMISTIC SPIN MODEL OF MAGNETISM

ternal factors also contribute to the energy of the spin system, such as Zeeman energy from magnetic field, Dzyaloshinskii-Moriya interaction from spin-orbit coupling, magnetic anisotropy from electrostatic crystal-field interaction and so on. The spin Hamiltonian is a summary of all mentioned energy contributions. The typical form of the spin Hamiltonian is:

$$\mathcal{H} = E_{ex} + E_{ani} + E_{app} + E_{DMI} + \dots \quad (2.1)$$

denoting terms of the exchange interaction, magnetic anisotropy, external magnetic fields, Dzyaloshinskii-Moriya interaction and other terms, e.g. dipole-dipole interaction.

2.1.2 General matrix expression of interaction

There are several equivalent forms of spin interactions, among which matrix form suit best with computational needs of the atomistic model. As the result of Heisenberg approach in quantum mechanics[23], the general interaction between two spins \mathbf{S}_i and \mathbf{S}_j can be written as:

$$\mathbf{S}_i^T \mathbf{J}_{ij} \mathbf{S}_j \quad (2.2)$$

where the full expression in three dimension x, y, z is

$$\mathbf{S}_i^T = \begin{bmatrix} S_x^i & S_y^i & S_z^i \end{bmatrix}, \mathbf{J}_{ij} = \begin{bmatrix} J_{xx} & J_{xy} & J_{xz} \\ J_{yx} & J_{yy} & J_{yz} \\ J_{zx} & J_{zy} & J_{zz} \end{bmatrix}, \mathbf{S}_j = \begin{bmatrix} S_x^j \\ S_y^j \\ S_z^j \end{bmatrix} \quad (2.3)$$

in which \mathbf{J}_{ij} is a 3×3 matrix elements mainly dependent on the position of spins and the lattice environment. The interaction matrix \mathbf{J}_{ij} contains both diagonal part, which is the isotropic exchange interaction, and off-diagonal part, in the case of this thesis is the Dzyaloshinskii-Moriya interaction. The interactions will be discussed in detail in the following sections.

2.1.3 Exchange interaction

The dominant term in the spin Hamiltonian is the exchange energy, which tends to align neighbouring spins in parallel or anti-parallel direction, giving rise to ferromagnetism or antiferromagnetism respectively. From quantum

mechanics, the exchange energy is defined as the energy difference between parallel and antiparallel spin-coupling, which is originated from the symmetry of the electron wavefunction and the Pauli principle[24]. In practice, the exchange energy could be calculated from DFT (Density Functional Theory) approach theoretically[25], or determined by fitting to experiments if the DFT calculations are not possible.

The Heisenberg exchange energy can be written as

$$E_{ex} = - \sum_{i \neq j} J_{ij} \mathbf{S}_i \cdot \mathbf{S}_j \quad (2.4)$$

where J_{ij} is the exchange constant between atomic site i and j , \mathbf{S}_i is a unit vector signify the local spin moment and \mathbf{S}_j is the neighbouring spin moment direction. In the matrix expression, J_{ij} is the isotropic diagonal part of \mathbf{J}_{ij} . A positive J_{ij} means parallel or ferromagnetic spin coupling whereas a negative J_{ij} means spins are antiparallel or antiferromagnetic. The positive J_{ij} is the concern of this thesis.

2.1.4 Magnetic anisotropy

The magnetic anisotropy brings in the preferred direction of atomic moment, which determines some important features of magnetic material such as hysteresis and coercivity[26]. Several physics effects are related to magnetic anisotropy, among which the main source is magnetocrystalline anisotropy. This results from electrostatic crystal-field interaction and relativistic spin-orbit coupling, and generates particular crystallographic axes preferred by spin moments[27].

The simplest form of anisotropy is single-ion uniaxial type[22], where the magnetic moments prefer to align along a single axis, \mathbf{e} , often called the easy axis. The corresponding anisotropy energy is

$$E_{ani}^{uni} = -k_u \sum_i (\mathbf{S}_i \cdot \mathbf{e})^2 \quad (2.5)$$

which k_u is the anisotropy energy per atom.

Cubic anisotropy is also a common type of magnetic anisotropy, which is generally smaller than uniaxial anisotropy. With three principal directions that

2.1. ATOMISTIC SPIN MODEL OF MAGNETISM

energetically rank from easy to hard, the cubic anisotropy is described by

$$E_{ani}^{cubic} = \frac{k_c}{2} \sum_i (\mathbf{S}_x^4 + \mathbf{S}_y^4 + \mathbf{S}_z^4) \quad (2.6)$$

where k_c is the cubic anisotropy energy per atom, and \mathbf{S}_x , \mathbf{S}_y and \mathbf{S}_z are the x , y and z components of the spin moment \mathbf{S} .

2.1.5 Applied field

The applied fields, denoted as H_{app} , are also involved in most studies of magnetic systems. The energy from applied fields is frequently called Zeeman energy, which comes from the local moments induced by applied magnetic fields. The applied field energy, or Zeeman energy is mainly given by

$$E_{app} = - \sum_i \mu_s \mathbf{S}_i \cdot \mathbf{H}_{app}. \quad (2.7)$$

2.1.6 Dzyaloshinskii-Moriya interaction

The off-diagonal term of the interaction matrix is called Dzyaloshinskii-Moriya interaction (DMI)[28][29]. The DMI is the major factor in creating skyrmion in this thesis. The origin of DMI is the inversion-asymmetric lattice environment and strong spin-orbit coupling.

There are several possible assemblies of magnetic thin films and metals with large spin-orbit coupling that leads to observable effect of DM interaction, including bilayers like Fe on Ir(111)[13] and Mn on W(110)[30], multilayers like Fe/Ni/Cu(001)[31], Pt/Ir/Co/Pt[32] etc.

The energy of DMI is always written in a way of spin cross product:

$$E_{DMI} = \mathbf{D}_{ij} \cdot (\mathbf{S}_i \times \mathbf{S}_j) \quad (2.8)$$

according to equation (2.8), the direction of such interaction exhibit a chiral property. The simplest example, as is shown in figure 2.1, is two dimension DMI in $x - y$ plane:

$$\begin{aligned} E_{DMI}^{12} &= \mathbf{D}_{12} \cdot (\mathbf{S}_1 \times \mathbf{S}_2) \cdot \mathbf{y} = \mathbf{D}_{12} \cdot (\mathbf{S}_1^z \mathbf{S}_2^x - \mathbf{S}_1^x \mathbf{S}_2^z) \cdot \mathbf{y}, \\ E_{DMI}^{13} &= \mathbf{D}_{13} \cdot (\mathbf{S}_1 \times \mathbf{S}_3) \cdot (-\mathbf{x}) = \mathbf{D}_{13} \cdot (\mathbf{S}_1^z \mathbf{S}_3^y - \mathbf{S}_1^y \mathbf{S}_3^z) \cdot (-\mathbf{x}) \end{aligned} \quad (2.9)$$

The equations (2.9) yield a matrix expression combining the DMI, together with the diagonal isotropic exchange:

$$\mathbf{J}_{12} = \begin{bmatrix} J_{xx} & 0 & -D_{xz} \\ 0 & J_{yy} & 0 \\ D_{zx} & 0 & J_{zz} \end{bmatrix}, \mathbf{J}_{13} = \begin{bmatrix} J_{xx} & 0 & 0 \\ 0 & J_{yy} & -D_{yz} \\ 0 & D_{zy} & J_{zz} \end{bmatrix} \quad (2.10)$$

Note that for real materials the DMI always exists in three dimensions and with different value[33].

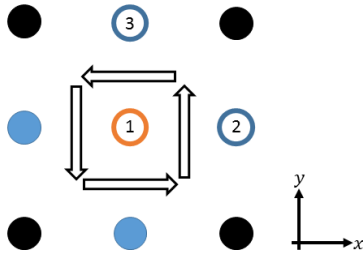


Figure 2.1: Simplified form of two dimensional DM interaction within neighboring atoms: atom 1 (orange circle) is interacting with four atoms (blue circles), of which directions are indicated by feint black arrows. Detailed equation of DM interactions between spin 1 & 2, 1 & 3 are given.

2.2 Atomistic spin dynamics

The spin Hamiltonian reveals the total energy of the spin system, however it cannot provide information about the time-dependent properties and the thermal effects. In this section, general spin dynamics equations including applied magnetic and thermal field are introduced.

2.2.1 Landau-Lifshitz-Gilbert equation

The basic form of time evolution of the spin moments in presence of an applied magnetic field is given by[34]

$$\frac{d\mathbf{S}(t)}{dt} = -\gamma_0[\mathbf{S}(t) \times \mathbf{H}(t)], \quad \gamma_0 = \frac{g\mu_B\mu_0}{\hbar} \quad (2.11)$$

2.2. ATOMISTIC SPIN DYNAMICS

where g, μ_B and μ_0 are the gyromagnetic ratio, Bohr magneton and vacuum permeability. The equation (2.11) is based on the derivation from expectation value of the spin according to the Schrodinger equation:

$$\frac{d\mathbf{S}(t)}{dt} = \frac{1}{i\hbar}[\mathbf{S}(t), \mathbf{H}(t)]. \quad (2.12)$$

A phenomenological damping term suggested by Gilbert[35] is added to describe the evolution of the magnetic spins to equilibrium with the field, which leads to the saturation of ferromagnetic materials with increasing applied magnetic field[36]. As a result, the spin dynamic equation can be shown as

$$\frac{d\mathbf{S}(t)}{dt} = -\gamma_0[\mathbf{S}(t) \times \mathbf{H}(t)] + \alpha\gamma_0[\mathbf{S}(t) \times \frac{d\mathbf{S}(t)}{dt}], \quad (2.13)$$

with the damping constant α illustrated by Kikuchi[37] that $\alpha = 1$ gives the highest switching speed of the ferromagnetic domains and in most cases $\alpha \ll 1$. After substituting equation (2.11) for $\frac{d\mathbf{S}(t)}{dt}$ and suitable rescaling of t in equation (2.13), the equation can be rewritten as

$$\frac{d\mathbf{S}}{dt} = [\mathbf{S} \times \mathbf{H}] + \alpha[\mathbf{S} \times [\mathbf{S} \times \mathbf{H}]], \quad (2.14)$$

which is the basic form of Landau-Lifshitz-Gilbert equation. In the atomistic model, the applied magnetic field H is substituted by the effective net magnetic field H_{eff}^i on each spin \mathbf{S}_i . The H_{eff}^i is obtained from the derivative of the total spin Hamilton

$$H_{eff}^i = -\frac{1}{\mu_s} \frac{\partial \mathcal{H}}{\partial \mathbf{S}_i}, \quad (2.15)$$

where μ_s is the local spin moment. Considering all the factors above, the atomistic Landau-Lifshitz-Gilbert equation is given by

$$\frac{d\mathbf{S}_i}{dt} = [\mathbf{S}_i \times \mathbf{H}_{eff}^i] + \alpha\mathbf{S}_i \times [\mathbf{S}_i \times \mathbf{H}_{eff}^i]. \quad (2.16)$$

2.2.2 Langevin dynamics

The fundamental form of LLG equation is valid only for zero temperature, which excludes thermal effects. To describe the spins dynamics under a finite temperature, Langevin dynamics can be taken into account. The analytic approach of Langevin dynamics is developed by Brown[38]. The basic idea

of the approach is to introduce a thermal noise term H_{th}^i into the effective magnetic field

$$H_{eff}^i = H_{th}^i + -\frac{1}{\mu_s} \frac{\partial \mathcal{H}}{\partial \mathbf{S}_i}, \quad (2.17)$$

with the thermal field obeys

$$\langle H_{th}^i \rangle = 0, \quad \langle H_i(t) H_j(t') \rangle = \delta_{i,j} \delta(t - t') 2\alpha k_B T \mu_s / \gamma, \quad (2.18)$$

where i, j denote the sites of the spins on lattice, and $\langle \rangle$ denotes an average value over realizations of the thermal field. The heat fluctuations on each spin are further assumed as independent random events with conditions in equation(2.18)[38], thus yield H_{th}^i represented by a Gaussian statistical distribution $\Gamma(t)$. Notice that the correlation time of H_{th}^i is much shorter than the rotational-response time due to $\delta(t - t')$ factor in equations(2.18)(white noise[39]). At small time step the instant thermal field on each spin located in site i is given by:

$$H_{th}^i = \Gamma(t) \sqrt{\frac{2\alpha k_B T \Delta t}{\gamma \mu_s}} \quad (2.19)$$

where Δt is the time integration step during the calculation. The thermal equation (2.19) is implemented into LLG equation, so that spin dynamics originated from both magnetic field and thermal field are considered in calculation, resulting in a stochastic LLG equation due to the random nature of thermal field.

2.2.3 Time integration

It is necessary to solve the LLG equation (2.21) with stochastic thermal term(2.17) within certain time step in order to simulate the time-evolving properties of the spin system. The Heun method[39] is widely used for the numerical study of the dynamics of magnetic materials. The predictor-corrector algorithm is applied in the method in order to obtain results using larger time steps, which presents sufficient accuracy and computational efficiency[22]. The first (predictor) step gives the new spin direction \mathbf{S}'_i under a given effective field H_{eff}^i by using a standard Euler integration step, given by:

$$\mathbf{S}'_i = \mathbf{S}_i + \Delta \mathbf{S} \Delta t \quad (2.20)$$

2.2. ATOMISTIC SPIN DYNAMICS

where the small change $\Delta \mathbf{S}$ is

$$\Delta \mathbf{S} = [\mathbf{S}_i \times H_{eff}^i] + \alpha \mathbf{S} \times [\mathbf{S}_i \times H_{eff}^i]. \quad (2.21)$$

The spin vector length should then be renormalized to the unit vector after each step to insure the stability and convergence of the solution. Also, the effective field needs to be recalculated for the second step due to the change in the spin configuration. The second (corrector) step uses assignments from the predicted spin direction \mathbf{S}'_i and re-evaluated effective field $H_{eff}^{i'}$ to calculate the final spin position, thus completing the whole integration step. The corrector equation is given by:

$$\mathbf{S}_i^{t+\Delta t} = \mathbf{S}_i + \frac{1}{2}[\Delta \mathbf{S} + \Delta \mathbf{S}']\Delta t \quad (2.22)$$

where the revised small change $\Delta \mathbf{S}'$ is

$$\Delta \mathbf{S}' = [\mathbf{S}'_i \times H_{eff}^{i'}] + \alpha \mathbf{S}' \times [\mathbf{S}'_i \times H_{eff}^{i'}]. \quad (2.23)$$

The predict-correct steps are applied on every spin with repeats many times so that the time evolution is simulated.

To compare of the calculated result with analytical solution, a simplified example is given in[22]. The analytical solution for time-depend evolution of a single spin originally along x axis with applied magnetic field in z direction is given by[2]:

$$\begin{aligned} S_x(t) &= \operatorname{sech}\left(\frac{\lambda\gamma H}{1+\lambda^2}t\right) \cdot \cos\left(\frac{\gamma H}{1+\lambda^2}t\right) \\ S_y(t) &= \operatorname{sech}\left(\frac{\lambda\gamma H}{1+\lambda^2}t\right) \cdot \sin\left(\frac{\gamma H}{1+\lambda^2}t\right) \\ S_z(t) &= \tanh\left(\frac{\lambda\gamma H}{1+\lambda^2}t\right) \end{aligned} \quad (2.24)$$

The analytical and computational time evolution for the model with $H = 10$ T, $\Delta t = 1 \times 10^{-15}$ s, and $\lambda = 0.1, 0.05$ is shown in figure 2.2, which indicates a good accordance.

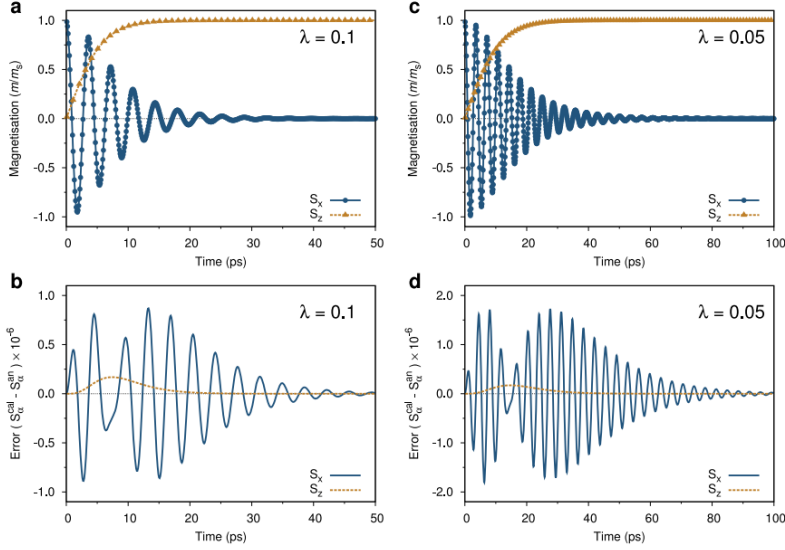


Figure 2.2: The analytical solution is plotted in the lines, comparing with the points for computational approach. Panel (b) and (d) illustrate the error traces for two damping constants for (a) and (c). The error is in the magnitudes of 10^{-6} , which shows good correspondence. Extract from [2].

2.3 Monte Carlo method

While spin dynamic methods generate good results over dynamic properties of magnetic systems, those methods are not well-suited for determining the equilibrium properties like the temperature-dependent magnetization. The Monte Carlo methods, however, have the advantage over the dynamics methods in evolving to equilibrium due to its statistical nature in finding energy-favored state.

According to classic statistical mechanics, the probability of n th state in the system can be written as

$$P_n = e^{E_n/k_B T} / Z \quad (2.25)$$

where Z is called the partition function calculated from all possible energy values:

$$Z = \sum_E e^{E_n/k_B T}. \quad (2.26)$$

The equilibrium properties can be obtained if Z is known, while it is almost impossible to obtain its exact value in most cases. As to find out the equilibrium

2.4. MAGNETIC SKYRMIONS

properties of a system without calculating the partition function, the Monte Carlo Metropolis algorithm[40] is applied as the calculation technique. In the algorithm, the transition probability from randomly chosen state to another is calculated instead of applying the partition function of a certain state. The normalized transition probability of two different energy of the state, namely E_1 and E_2 , follows the Boltzmann distribution:

$$P_{1-2} = \exp\left(-\frac{\Delta E}{k_B T}\right). \quad (2.27)$$

Thus, the partition function (2.26) is omitted in the calculation steps.

The basic procession of the Metropolis algorithm works as following:

- (1) Initialize a net spin state,
- (2) Pick a random spin \mathbf{S}_i and randomly change the spin direction to \mathbf{S}'_i ;
- (3) Calculate the energy change $\Delta E = E(\mathbf{S}'_i) - E(\mathbf{S}_i)$;
- (4) Calculate the probability P by (2.27), if $P > 1$, which means reduction in energy by the change, then accept the motion;
- (4) Generate a random number r in the range $0 < r < 1$,
- (5) Compare r with P , if $P > r$, accept the motion;
- (6) Go to next site and process from (3) until covering complete the spins of the system.

After the complete spins being considered, the properties of the system in its lowest energy are determined. In addition, statistical average can be obtained by looping the calculation procedure several times to rise the accuracy.

2.4 Magnetic skyrmions

2.4.1 Definition of skyrmions

Skyrmions are named after the particle physics theorist Tony Skyrme who developed a nonlinear field theory[3] to describe interacting mesons and baryons in the topological perspective. Originally related to particle-like solutions, skyrmions are now used to identify similar structures in varied contexts, e.g., quantum Hall systems[41][42], Bose-Einstein condensation[43][44] and liquid crystals[45].

In general, skyrmions are vector fields with a spherical topology characterized by topological charge, usually called the topological skyrmion number N_{sk}

$$N_{skr} = \frac{1}{4\pi} \iint dx dy \mathbf{n} \cdot \left(\frac{\partial \mathbf{n}}{\partial x} \times \frac{\partial \mathbf{n}}{\partial y} \right) \quad (2.28)$$

as the surface integral of unit vector \mathbf{n} over the plane denoted by x and y . Therefore, when vector texture varies continuously in all directions, i.e. \mathbf{n} wraps around a unit sphere, the N_{skr} is equal to 1. In other word, a single skyrmion contributes one to the topological skyrmion number, which means skyrmions can be clearly counted in an ordered state. As a result, the topological skyrmion number can be applied to wherever skyrmion-like structures emerge to analyze their topological properties. This concept remains valid for magnetic skyrmions by calculating the skyrmion number over the discrete lattice (Appendix A), which are the concern of this thesis.

2.4.2 Physical origins of magnetic skyrmions

In magnetic materials, the skyrmion state emerge as particle-like excitations which lies between spiral state and ferromagnetic state. Any broken symmetry of the lattice with chiral character could lead to skyrmion state. There are several mechanisms giving rise to the magnetic skyrmion formation:

- (1) Four-spin exchange, resulting in superposition of spin spirals in shaping skyrmions[13],
- (2) Dzyaloshinskii-Moriya interaction, giving rise to chiral interaction among neighboring spins so that a skyrmion lattice nucleates under magnetic field,
- (3) Dipole-dipole interaction, stabilizing large skyrmions with a diameter of the order of μm [46],
- (4) Frustrated exchange interactions, maintaining both skyrmions and anti-skyrmions[47].

Among four mechanisms mentioned above, the Dzyaloshinskii-Moriya interaction and the Dipole-Dipole interaction attract most research interests. The size of skyrmions by Dipole-Dipole interaction is much larger (10^2) than skyrmions by DMI. Due to the nature of our atomistic spin model, there will be excessive CPU requirements for calculating quantity of a system with the length of

2.4. MAGNETIC SKYRMIONS

micrometer or above. As a result, the DMI type skyrmion with the scale of nanometer is focused in the computational research presented here.

2.4.3 Summary

In this chapter, the physics basis of a magnetic system is introduced, including the Heisenberg Hamiltonian for total energy and LLG equation for dynamic properties. The computational methods are described, including Heun method for LLG equation time integration and Monte-Carlo method for the equilibrium properties. Additionally, the meaning of a skyrmion is explained, followed by basic information about the magnetic skyrmions.

The next chapters will focus on the nucleation conditions and the phase diagram of magnetic skyrmion lattice.

Chapter 3

Existence Criteria for the Skymion Phase at 0 K

This chapter focuses on nucleation of the skyrmion lattice in the magnetic thin film. For the purpose of systematic study on the basic nucleation conditions, the models in use are simplified in several ways. Firstly, the magnetic film is set to be a monolayer so that the skyrmion lattice is confined into two-dimensions. Secondly, the applied magnetic field is assumed to be perpendicular to the lattice plane. Thirdly, the equilibrium temperature of the lattice is set to be 0K, and the thermal effect will be studied in next chapter.

In this chapter, an example of the skyrmion lattice will be introduced first, followed by controlled studies on various parameters. The material properties will be set invariant first so as to investigate the effect of the magnetic field on the lattice and the changes when the field is removed. Then the material parameters such as the exchange energy, DM interaction and magnetic anisotropy are modified to illustrate their influence on the spin configuration.

3.1 Example of skyrmion lattice

An Example of the ideal skyrmion lattice is illustrated in this section. The basic requirements of nucleating a skyrmion lattice include the ferromagnetic exchange interaction and the DM interaction , with adequate perpendicular magnetic field.

3.1. EXAMPLE OF SKYRMION LATTICE

The parameters of this model and the simulation procedure are set as follows. The exchange interaction and the DM interaction are equally set as 1 meV, allowing the size of a single skyrmion to be around 2 nm. In that case the critical magnetic field for the skyrmion state is 3.2 T. The two-dimensional monolayer consists of the simple cubic lattice with the lattice constant 2.715 Å. The geometry of the system is square with 32 lattice site each side (8.688 nm). The procedure of the nucleation follows linear field-cooling with constant magnetic field applied, as is shown in figure 3.1.

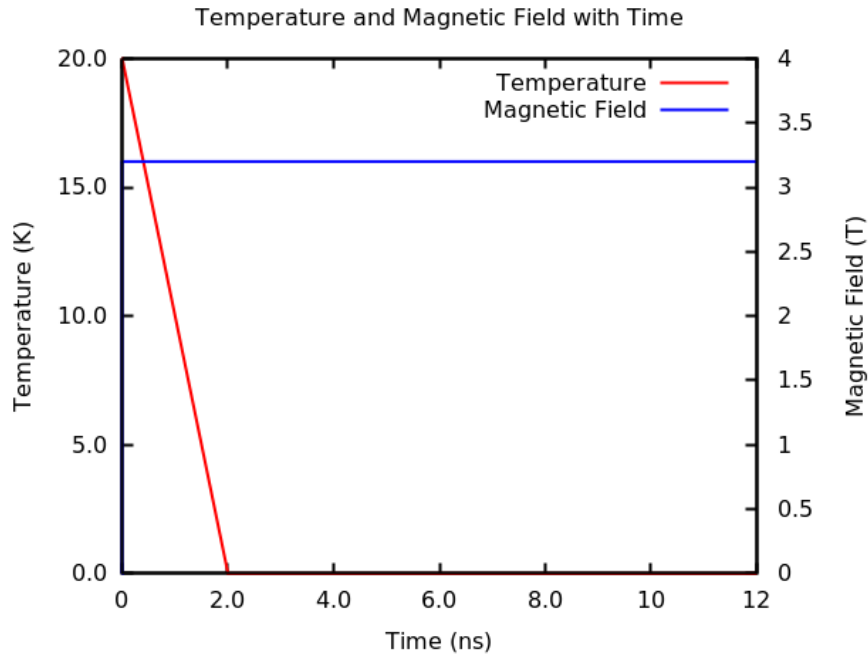


Figure 3.1: The thermal field-cooling in red line starts from 20K, cooling to 0K in 2ns. The constant magnetic field of 3.2 T is shown as the blue line.

The system can be considered fully relaxed in 10 ns in 0 K, followed by 2 ns cooling. This procedure forms ground state of the lattice at 0 K with 3.2 T magnetic field. The snapshot of the system, which gives clear vision of the spin configuration, is shown in figure 3.2.

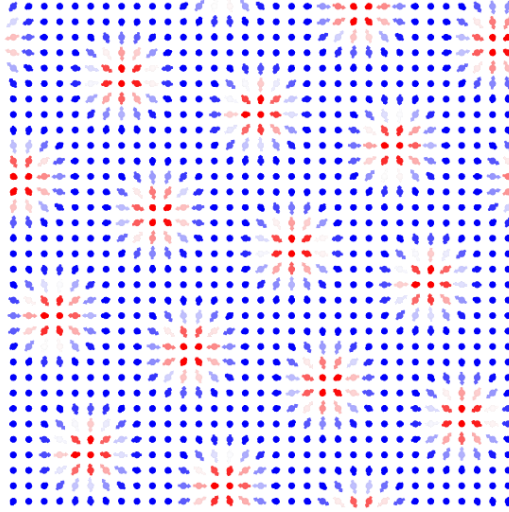


Figure 3.2: The spins are represented by colored arrows, where the color scale linearly depends on their value in z -component, with blue for -1 and red for $+1$. The skyrmion structure is clearly shown in the whole lattice with an hexagonal structure.

The given example shows a perfect skyrmion lattice with controlled conditions for the simplified model outlined earlier, including the exchange interaction, the DM interaction and the magnetic field with field-cooling. The effect of those parameters will be studied quantitatively in the following sections.

3.2 Constant material parameters

In this section, the parameters of the material will be kept constant, as follows:

- 1) the exchange constant $J= 1$ meV,
- 2) DM interaction $D= 1$ meV,
- 3) the atomic spin moment $\mu_s= 2.7 \mu_B$,
- 4) the damping $\alpha= 0.05$,
- 5) lattice constant $a= 2.715 \text{ \AA}$,
- 6) size 32×32

Although the DM interaction is always less than the exchange interaction in real materials, the ratio of D and J merely influence on the critical magnetic field and the size of skyrmion in our model (discussed in detail in section **3.3.1**).

3.2. CONSTANT MATERIAL PARAMETERS

In order to improve the efficiency of the simulations with small skyrmions, the ratio here is kept to be 1 initially. Noting that the anisotropy is not considered in this section.

3.2.1 Spin states with varied magnetic field

The effect of different magnetic fields on spin states will be discussed first. The cooling procedure is the same as shown in figure 3.1. The applied magnetic field is varied from 0 T to 6 T with a step of 0.2 T. The states of the system are identified by three parameters, as is shown in figure 3.3 : the total energy, the skyrmion number and the magnetization.

The total energy indicates the stability of the states, specifically more stable in lower energy. The skyrmion number shows how many skyrmion-like spin structures exist in the lattice. The magnetization of the system rises almost linearly with the magnetic field, indicating the material behaves with constant susceptibility similar to a paramagnet[24]:

$$M = \chi_m H, \quad (3.1)$$

where χ_m is called magnetic susceptibility. As is expected, the magnetization saturates for large magnetic field, 5.4 T in this case. The total energy and the skyrmion number of the system shows different trends in several ranges with magnetic field, arising from the evolution of the spin states. The skyrmion number, for example, remains zero from 0 T to 0.6 T, thus no skyrmions are nucleated. Then in the range of 0.8 T to 1.4 T the structure consists of a mixture of spiral states with sporadic skyrmions. In the range 1.6 T to 4.2 T, the skyrmion number fluctuates between 10 and 13, illustrating a well-nucleated skyrmion lattice. A decrease of skyrmion number in the range 4.4 T to 5.4 T indicates the system entering into ferromagnetic states however with some surviving skyrmions. Finally the skyrmion number returns back to zero as the system becomes totally ferromagnetic. The variation of the energy shows similar trends to the skyrmion number. Those states are specified by the states **(a)**-**(e)** in the figure, while the classification of these five ranges will be shown clearly by their spin figures in the ensuing paragraphs.

3.2. CONSTANT MATERIAL PARAMETERS

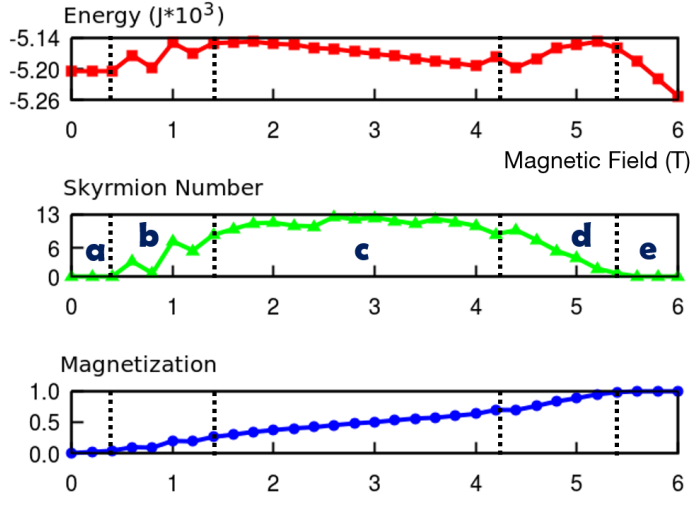


Figure 3.3: The total energy, skyrmion number and magnetization of each spin states, divided as **a-e** in the figure.

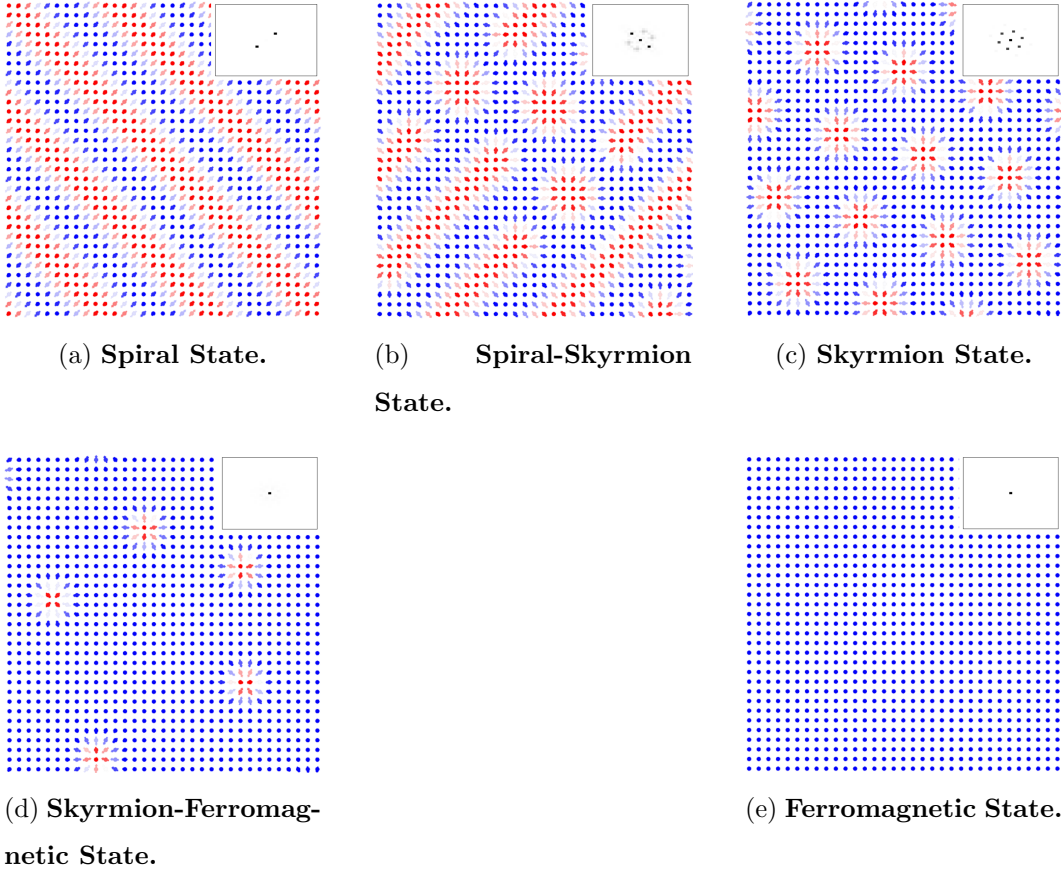


Figure 3.4: (a)-(e): five spin states under varied range of perpendicular magnetic field. Top-right part in each figure is the spin state in the momentum space.

3.2. CONSTANT MATERIAL PARAMETERS

In order to illustrate the long-range order, the spin states are transferred in to the momentum space by applying Fourier transform (FT) to the spins in the real space:

$$\mathbf{S}_k = \sum_j \mathbf{s}_j \exp(ik \cdot j), \quad (3.2)$$

\mathbf{S}_k indicates the vector of the spin in the momentum space and \mathbf{s}_j in the real space, while k and j indicate the position of the spin in momentum space and real space respectively. In the case of two-dimensions square lattice, the coordinate in momentum space is $k = \frac{2\pi}{j}$.

Spiral state : 0 T - 0.6 T

The ground state of the system with relatively low and no magnetic field is called the spiral state due to its spin configuration. The DMI and exchange interaction together shapes the stripe in absence of magnetic and thermal field[48]. The strip period of the spiral state is 2.1 nm. The FT diagram indicates the stripes has a transitional symmetry along diagonal direction.

Spiral-skyrmion state : 0.8 T - 1.4 T

With increasing magnetic field, some spins begin reversing from spirals pointing oppositely to the magnetic field, thus breaking the spiral state and nucleating skyrmions locally. The state of mixed spin configurations is called spiral-skyrmion state. The FT diagram indicates the broken transitional symmetry of the system in this state.

Skyrmion state : 1.6 T - 4.2 T

The skyrmion spin state nucleates after all the stripes anti-aligned to the magnetic field transform to the skyrmions in certain range of magnetic field. In a given skyrmion, spins are pointing in the direction of the magnetic field away from the skyrmion center, while pointing reversely at the core. The diameter of one skyrmion is approximately the same as the stripe period, which is 2.1 nm. The main character of the skyrmion distribution on the lattice is the hexagonal pattern in the FT diagram, which means a six-fold rotational symmetry of the lattice.

Skyrmion-ferromagnetic state : 4.4 T - 5.4 T

As the magnetic field increases further, the skyrmions begin to vanish as the central spins reverse into the field direction. The existing skyrmions shrink in size and become randomly distributed on the lattice. As is shown in the FT diagram, the rotational symmetry of the skyrmion phase is broken.

Ferromagnetic state : 5.6 T - 6 T

The magnetization of the system is saturated when the magnetic field is large enough, thus turning the spin system into the ferromagnetic state with all spins pointing to the direction of the magnetic field. The system possesses the same translational symmetry with a 2-dimension ferromagnetic square lattice.

The above-mentioned five states are the spin states under certain ranges of magnetic field at zero temperature. Among those states, the skyrmion state is the main concern of this thesis.

3.2.2 Spin states without magnetic field

The stability of spin states obtained under constant field is tested after removal of the magnetic field. The cooling procedure in figure 3.1 is kept the same, while the magnetic field is switched off after cooling down to 0 K, as in the figure 3.5. The spin states are thus created initially, prior to the removal of the magnetic field. In order to examine the properties of spin states at 0 T, their energy, skyrmion number and spin configuration are compared with the constant field case.

3.2. CONSTANT MATERIAL PARAMETERS

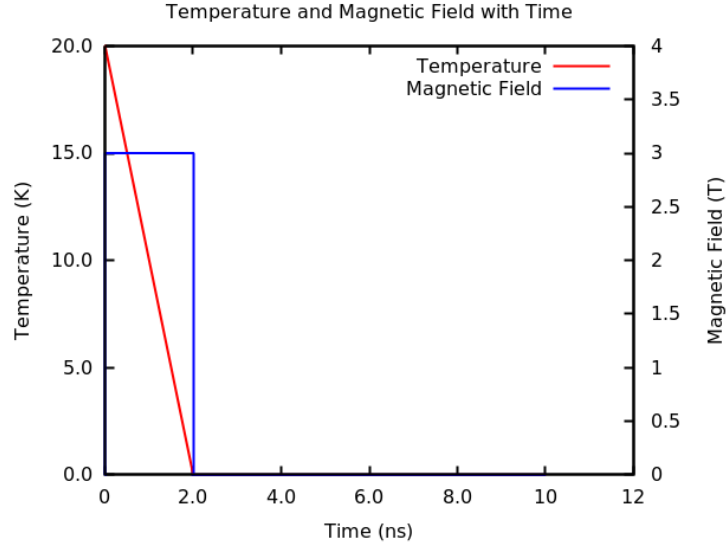


Figure 3.5: The thermal field-cooling in red line still starts from 20 K, cooling to 0K in 2 ns. The constant magnetic field is cutoff once field-cooling finished, as the blue line in 3.0 T.

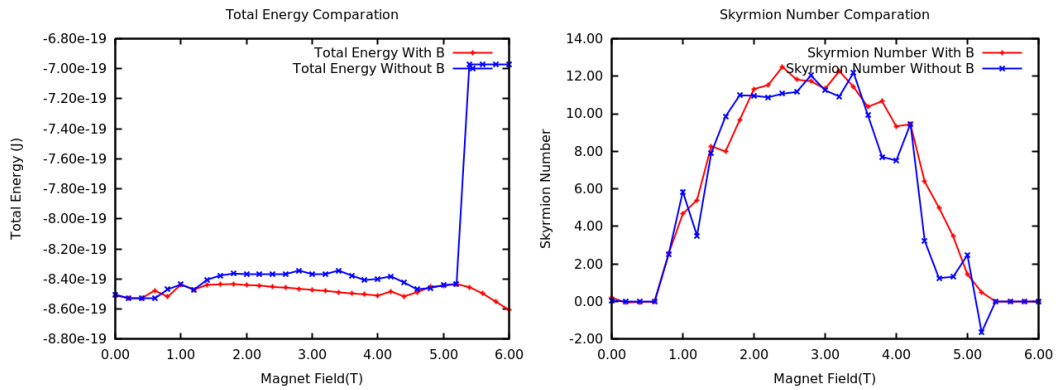


Figure 3.6: The comparison shows roughly the same skyrmion number with and without magnetic field, indicating the topological stability of the skyrmions. The total energy become higher in skyrmion states without magnetic field, while ferromagnetic state without the magnetic field is extremely unstable.

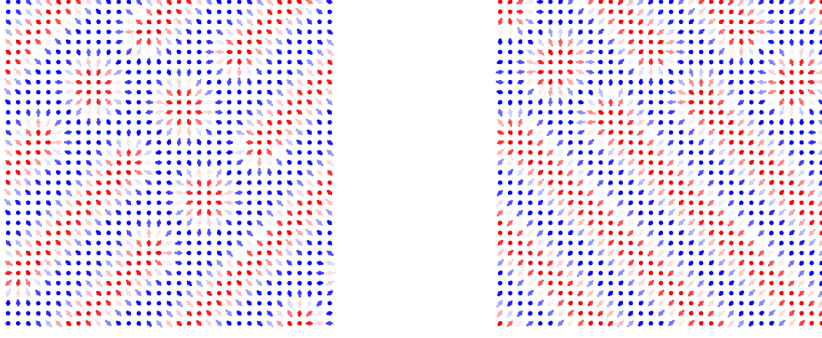


Figure 3.7: In the **b: Spiral-Skyrmion State**, some of the skyrmions still survive, while some vanish to form part of a stripe.

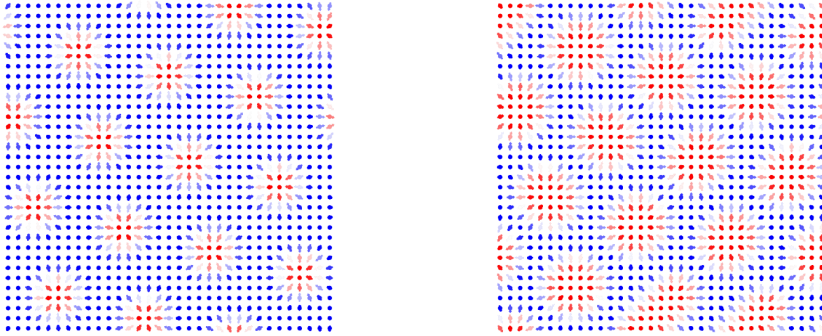


Figure 3.8: In the **c: Skyrmion State**, the skyrmions collectively enlarge without the magnetic field.

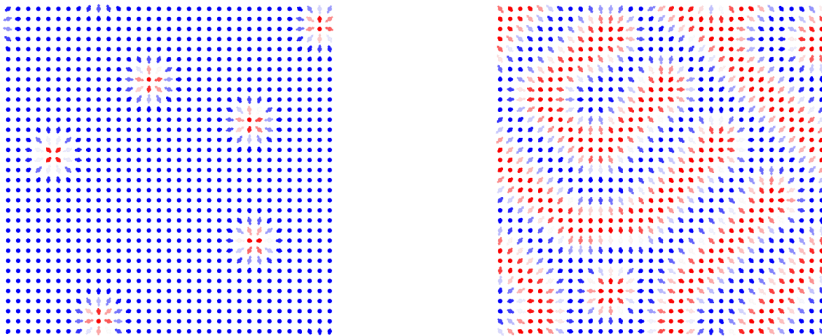


Figure 3.9: In the **d: Skyrmion-Ferromagnetic State**, the spin configuration becomes a mixture of mainly stripes with a randomly distributed skyrmion.

When the magnetic field vanishes, the spin system tends to turn back to

3.3. VARIED MATERIAL PARAMETERS

the spiral state due to the DM interaction. From the spin states **b,c and d** this trend is obviously observed as more stripes appearing and the skyrmions expanding. It is obvious that the stripes arise without the magnetic field since the spiral state is the ground state of zero temperature and no magnetic field. The enlargement of the skyrmions is also due to the trend in forming stripes. Meanwhile, the skyrmion structure is still preserved with expanding, so that their topological number remains almost the same, as is shown in Fig.3.6. The stability originates from the topological protection[14] that gives rise to an energy barrier between the skyrmions and other spin states with skyrmion number $N_{skr} \neq 1$. The skyrmions are stable against a certain range of external changes, specifically the disappearance of magnetic field in this case. The ferromagnetic state, on the other hand, retains its structure under the removal of the magnetic field. This invariance is due to the nature of the DM interaction. The DM interactions between the spins in this thesis are in-plane, as shown in figure 2.1. Given all the spins point vertically to the plane, nothing but S_z exist, and the in-plane DM interactions in x and y direction vanishes. This case, however, is a ideal unstable system not found in the real world because the temperature will never reach absolute zero and freezing the spin perfectly in z direction. Once small fluctuation due to thermal effect appears, the x and y components of the spin arise simultaneously, so that the DM interactions revive to affect the spin state.

3.3 Varied material parameters

The spin states at 0 K with certain material parameters have been studied in the previous section. The material parameters will be systematically modified in this section. The effect of changing critical DM interaction D and the exchange interaction J in absence of the anisotropy will be discussed first, including their influence on the skyrmion size and the magnetic field for nucleating the skyrmion state. Then the role of anisotropy is generally described with fixed D and J . The lattice constant and the size of the system in this section remain the same as in last section, and the studies focus on the skyrmion

state.

3.3.1 DM interaction and exchange interaction

The exchange interaction J and the DM interaction D are the building blocks of the skyrmion. To turn the spin state into the skyrmion state, the external magnetic field B need to be adjusted to different D and J . The relationship between B with D and J of the skyrmion state for certain lattice obeys an empirical equation [49]:

$$\mu_B B = cD^2/J, \quad (3.3)$$

where μ_B is the Bohr magneton, and c is the constant determined by inherent properties of lattice such as lattice constant, lattice crystallography, etc. The c in the paper[49] ranges from 0.23 to 0.78, while in the system of this thesis $c \approx 0.2$. On the other side, the size of one skyrmion can be defined by the diameter in pitch length of the lattice p [50].

$$D/J = \tan(2\pi/p). \quad (3.4)$$

The equation 3.3 with $c = 0.2$ is tested by two cases:

- i) fix $D = 1$ while $J = 1, 2, 3, 4$ and 5 (meV),
- ii) fix $D = 1$ while $J = 1, 2, 3, 4$ and 5 (meV).

The magnetic field B is calculated accordingly by (3.3), and the skyrmion diameter as pitch length is counted on the spin figures and compared with the equation (3.4).

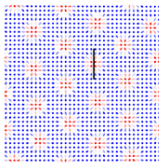
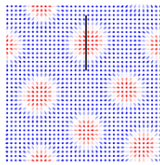
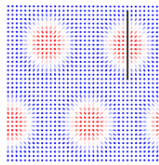
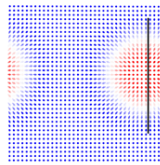
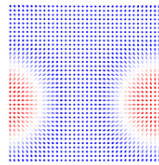
DM energy $D = 1$ meV					
Exchange energy J	1 meV	2 meV	3 meV	4 meV	5 meV
Magnetic field B	3.5 T	1.7 T	1.2 T	0.9 T	0.7 T
Pitch length p	8	13	16	27	30

Figure 3.10: The DM interaction D is fixed to be 1 meV, and the exchange interaction J ranges from 1 meV to 5 meV. The magnetic field B shown above is calculated from (3.3) with $c = 0.2$. The solid line on the spin figures demonstrates the pitch length of the skyrmion diameter.

3.3. VARIED MATERIAL PARAMETERS

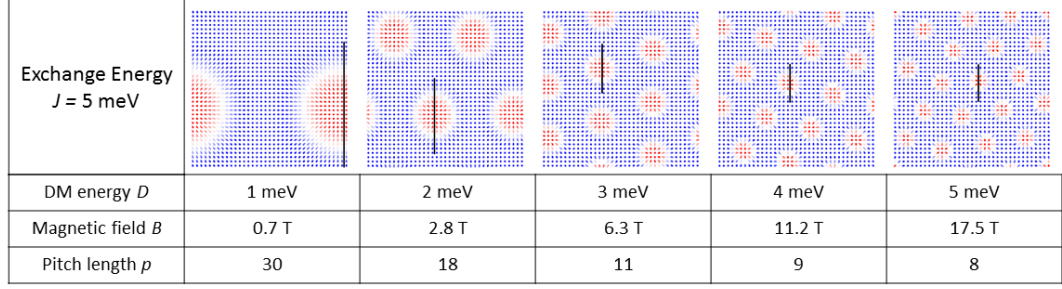


Figure 3.11: The exchange interaction J is fixed to be 1 meV, and the DM interaction D ranges from 1 meV to 5 meV. The magnetic field B is calculated from (3.3) with $c = 0.2$. The solid line on the spin figures demonstrates the pitch length of the skyrmion diameter.

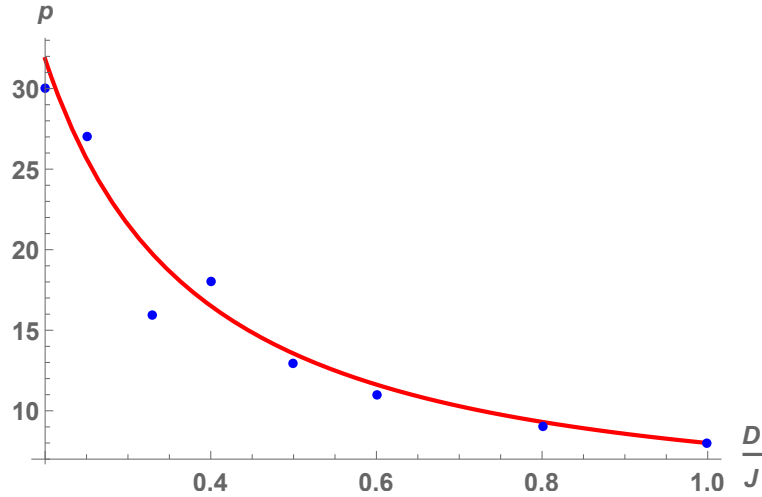


Figure 3.12: The theoretical size curve (red line) 3.4 and the counted size (blue point) are plotted together. p is the pitch length of the skyrmion diameter. The two values show a good accordance.

The magnetic field B is derived from equation (3.3) with $c = 0.2$, which fits well with the skyrmion state, as is shown in the spin figures in 3.10 and 3.11. Thus the ratio D^2 over J decides the required external field for the skyrmion phase. The diameter of the skyrmion, as measured in the spin figures, show good accordance with the theoretical derivation in figure 3.12.

3.3.2 Magnetic anisotropy

The connection between magnetic anisotropy and the properties of the skyrmion covers a large range of investigations[51][52]. The study here concentrates on the existence range of the skyrmion in varied anisotropy, both easy-axis and easy-plane, with fixed exchange interaction $J = 1$ meV and DM interaction $D = 1$ meV. The anisotropy ranges from -2.0 (easy axis) to 2.0 (easy plane) in step of 0.1, with the constant magnetic field sweep from 0 T to 10 T in step of 0.25 T. The creation procedure is the same as figure 3.1, and the size of lattice is kept at 32×32 . The skyrmion number of the material is calculated in each step.

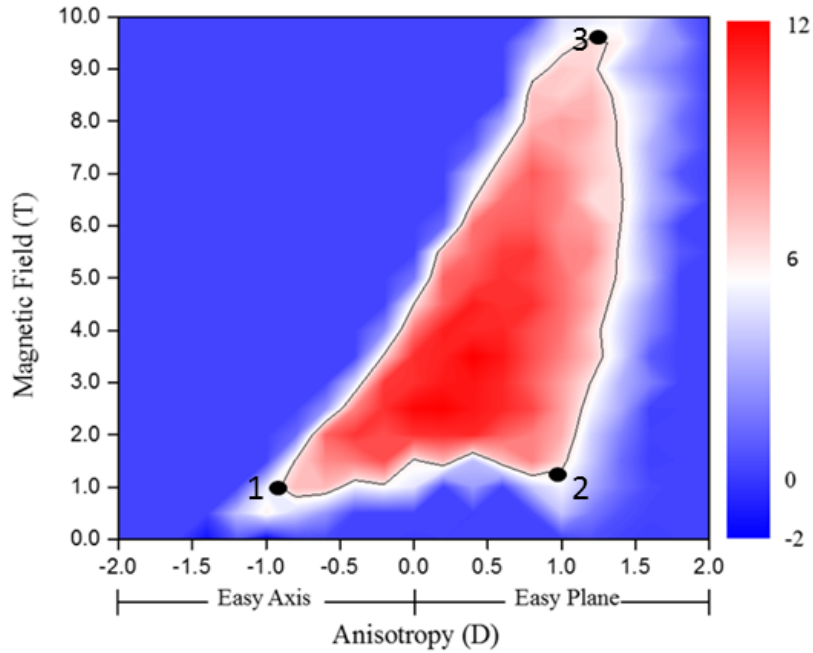


Figure 3.13: The contour plot consists by the skyrmion number as a function of the anisotropy and the magnetic field. The solid line indicates the skyrmion number of 6, which is nearly the half of the maximum number. Spin figures of three vertices of this triangle-like range are chosen to illustrate the magnetic configurations in the next figure, as shown by black dots in the plot: 1.(-1,1); 2.(1,1); 3.(1,9.5).

3.4. SUMMARY

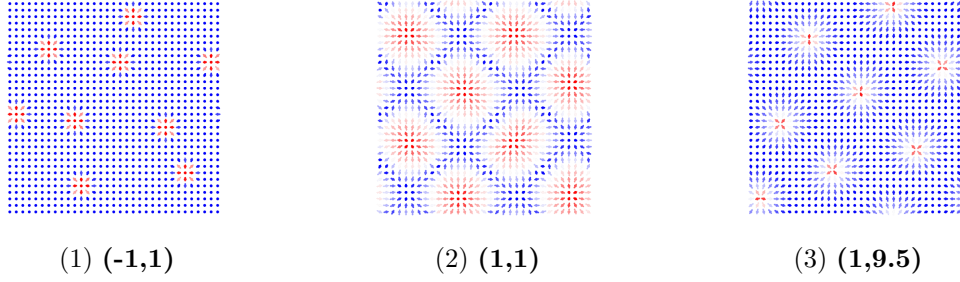


Figure 3.14: (1): with 1 meV easy axis anisotropy and 1 T perpendicular magnetic field, the skyrmions shrink significantly and disperse on the lattice, similar to the skyrmion-ferromagnetic state. (2): with 1 meV easy plane anisotropy and 1 T perpendicular magnetic field, the skyrmions enlarge in the shape of square. (3): with 1 meV easy plane anisotropy and 9.5 T perpendicular magnetic field, the ordered skyrmions still exist on lattice in large field.

Half of the maximum skyrmion number on lattice is set as the boundary of the general skyrmion state with other states. As shown in the figure, easy-plane anisotropy helps stabilizing the skyrmion in a larger range of external field because the the in-plane energy contribution serves to enhance the in-plane DM interaction, while the easy-axis anisotropy reduces the existence range due to the out-of-plane energy contribution that enhances the effect of the out-of-plane magnetic field. The shape of the skyrmion is modified by the anisotropy combining with different magnetic field.

3.4 Summary

In this chapter, the properties of the skyrmion lattice, especially in the skyrmion state are studied at 0 K. The relationship between magnetic field and spin states are demonstrated, and the stable spin states without magnetic field are illustrated. The material parameters, the exchange interaction J , the DM interaction D and the anisotropy A are studied separately to show their influence on the skyrmion state.

In the next chapter, the thermal effect will be studied in detail for the skyrmion state.

Chapter 4

Thermal Phase Diagram of the Skyrmion Lattice

The thermal stability of the topological spin state in the two-dimensional lattice is a complicated theoretical problem. The common parameters, such as the magnetization and the total energy, vary continuously with temperature (figure 4.1) and do not define the phase boundaries. In this chapter, a quantitative description of the thermal skyrmion phase diagram is obtained by the study of the spin figures of the skyrmion state, combined with several derivative parameters from the simulations.

The general phase diagram of the skyrmion lattice with perpendicular magnetic field and temperature will first be developed as a general basis of further discussion. The perpendicular magnetic field of 3.2 T is maintained in the following sections, which leads to a perfect hexagonal skyrmion lattice at 0 K as the ground state. Temperature is varied in order to obtain the thermal stability of the skyrmions. Several parameters are introduced to define the thermal stability of the skyrmion state, including the static magnetic susceptibility, the specific heat capacity and the skyrmion life time. Finally, the phase diagram of the skyrmion state is calculated numerically.

The material parameters are set as the same in Section 3.2.

4.1. EQUILIBRIUM PHASE DIAGRAM

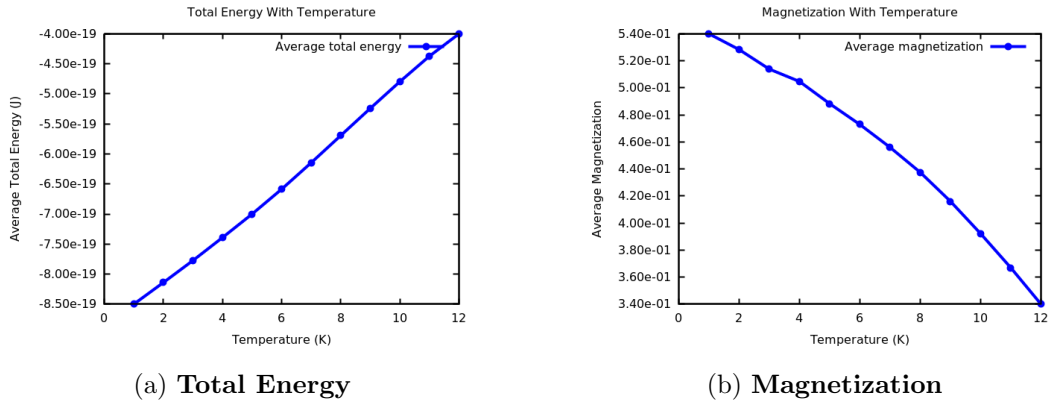


Figure 4.1: The total energy and magnetization with temperature: each point is calculated as the average value over several nanoseconds in thermal equilibrium. The two parameters change continuously with increasing temperature.

4.1 Equilibrium phase diagram

The general phase diagram of the lattice is an equilibrium contour plot of the skyrmion number N_{skr} over perpendicular magnetic field B and temperature T . For each data point of the plot, the lattice is fully relaxed after an equilibrium time of 10 ns with a given magnetic field and temperature, and the skyrmion number is calculated from each point. The magnetic field ranges from 0 T to 6 T with a step of 0.1 T, and the temperature 0 K to 15 K with step of 0.25 K. The plot is thus made up by 60×60 data points.

At 0 K, the phase diagram is a plot of the results in the previous chapter and shows that the skyrmion state emerges in the perpendicular magnetic field in the range 1.6 T to 4.2 T. A skyrmion number $N_{skr} \geq 6$ indicates the boundary of the skyrmion state, both for zero and non-zero temperature. The thermal stability of the skyrmion state also varies with the magnetic field, and the maximum temperature for stability of the skyrmion state is around 6 K in around 3 T magnetic field.

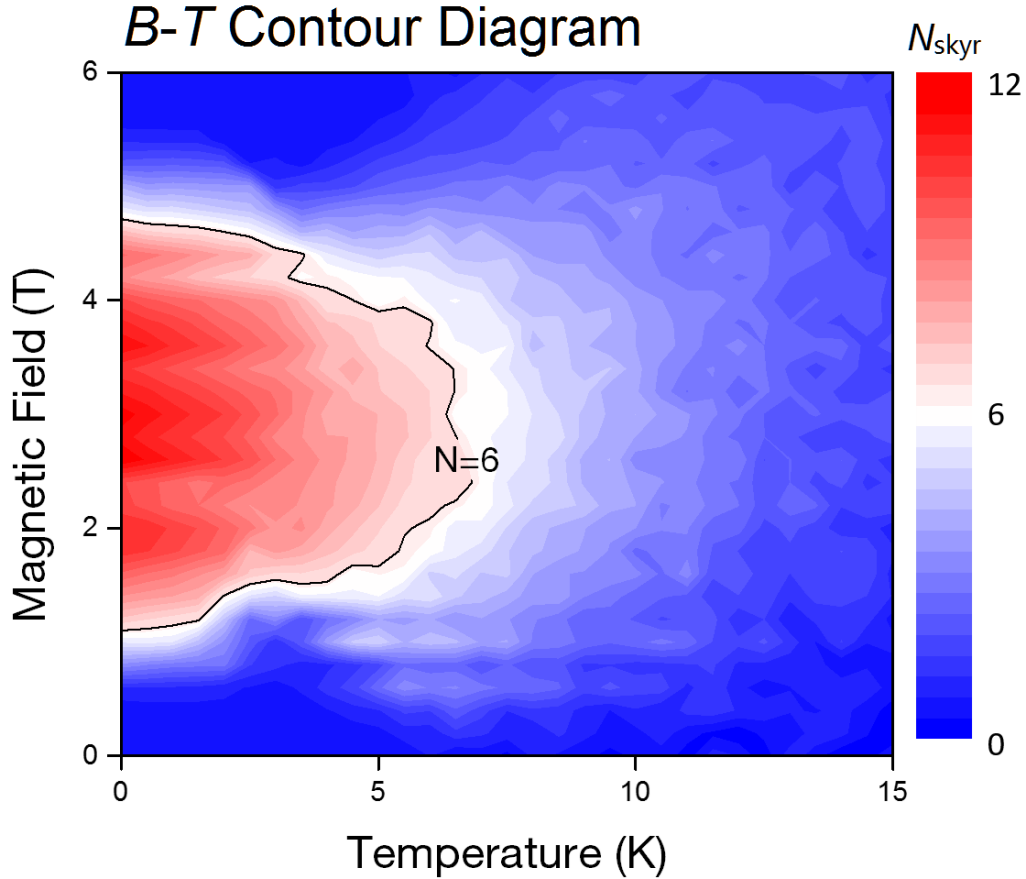


Figure 4.2: The contour diagram is consisted by the skyrmion number over temperature and perpendicular magnetic field. The color bar on the right side shows the magnitude of the skyrmion number. The solid line indicates a skyrmion number of 6, which is half of the maximum skyrmion number of the lattice.

4.1.1 Topological energy barrier

The topological energy barrier of the skyrmion structure is the most interesting property of the skyrmions. In the case of the lattice under the magnetic field at non-zero temperature, the two fields exert different effects on the skyrmion lattice. The magnetic field tends to create and maintain the skyrmion structure, while the thermal field damages the ordered spin state. Therefore, if the skyrmion lattice is to be stable when the thermal field is higher than the magnetic field, an energy barrier E_B must be introduced to stabilize the topo-

4.1. EQUILIBRIUM PHASE DIAGRAM

logical structure.

One could estimate this intrinsic energy barrier E_B by applying thermal field on the skyrmion state in zero field, which has been discussed in section 3.2.2. In this case, the energy barrier serves as an unique factor to protect the skyrmion structure. For a simple estimate, it can be assumed that the skyrmion energy barrier will not change in different temperatures. Therefore, by scanning the equilibrium skyrmion number of the lattice as a function of temperature, the critical temperature of skyrmion annihilation can be found, and the estimated energy barrier is equivalent to the thermal energy at this critical temperature. As is shown in Fig. 4.3, the critical temperature of the skyrmion annihilation is around 1 K. We estimate the zero field energy barrier from the critical temperature T_{crit} as follows:

$$E_{b0} = k_B T_{crit}, \quad (4.1)$$

where k_B is the Boltzmann constant.

Given that $T_{crit} = 1$ K, the energy barrier can be estimated as 10^{-1} eV from equation (4.1) for the whole lattice.

Then the value of E_b in the magnetic field can be applied in estimating the critical temperature with 3.2 T magnetic field for the skyrmion spin state:

$$E_{b(H)} = E_{b0} + E_m, \quad (4.2)$$

The energy of the magnetic field can be expressed as $E_m = \mu_B H$, so that the estimated temperature for phase transition in 3.2 T is around 6 K, which is consistent with the general phase diagram.

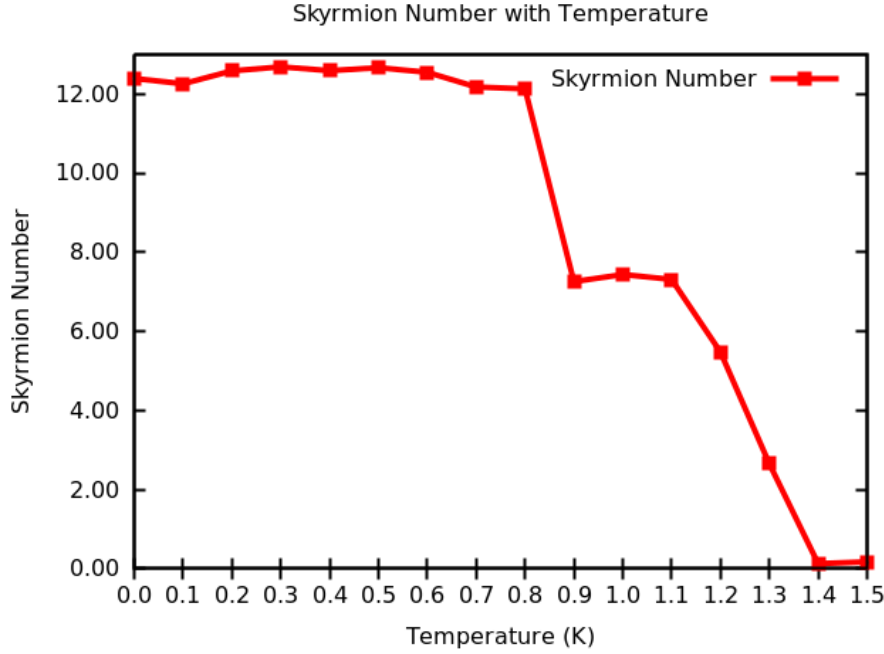


Figure 4.3: The skyrmion number of the skyrmion lattice without magnetic field: the skyrmion number here is calculated at thermal equilibrium at each temperature. The skyrmion structure stabilizes below 0.8 K, and experiences a transitional phase in range of 0.9 K to 1.3 K. The topological structure is totally broken at 1.4 K and above.

Based on the contour plot and an estimated value, the critical temperature for skyrmion annihilation lies at 6 K. In following sections, the skyrmion state in 3.2 T will be studied under varying temperatures and the estimated critical temperature 6 K will be further examined.

4.2 Analysis of spin figures

In order to examine the phase transition of the skyrmion lattice, the spin figures in real and momentum space at different temperatures are studied first, giving insight into the lattice behavior in the thermal field. The deformation of the skyrmions in low temperature and the interaction in higher temperature are then shown in order to illustrate their behavior in different temperature regions.

4.2. ANALYSIS OF SPIN FIGURES

4.2.1 Spin figures in real and momentum space

In order to examine the phase transition of the skyrmion lattice, the spin figures in real and momentum space at different temperatures are studied first, giving an insight into the lattice behavior in the thermal field.

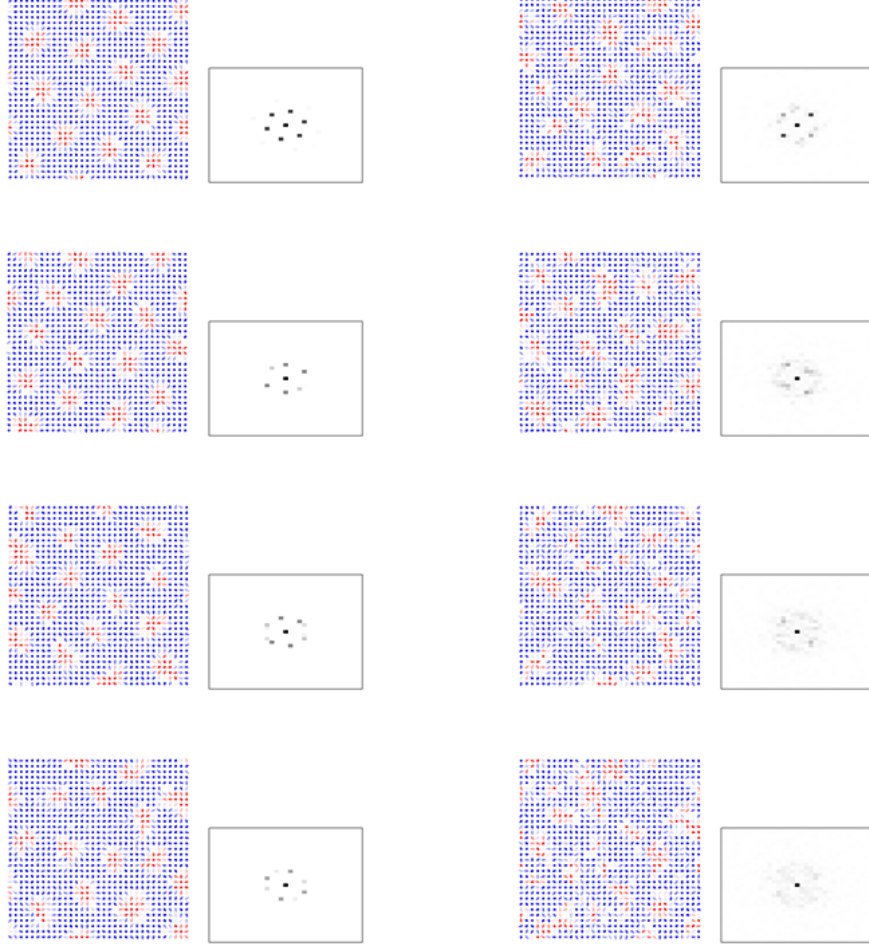


Figure 4.4: The real-space spin figures and Fourier intensity at 1-8 K. The central peak ($k = 0$) is the largest value in the momentum space. The Fourier points are scaled with gray level, i.e white as zero and black represents the largest value. Left column from top: $T = 1$ K, 2 K, 3 K and 4 K; right column from top: $T = 5$ K, 6 K, 7 K and 8 K.

In Fig.4.4, example spin states in thermal equilibrium at different temperatures are shown with the Fourier diagram, between $T = 1$ K and 8 K. The lattice symmetry in momentum space remains obvious below about 5 K, while at 6 K the symmetry is compromised with peaks beginning to merge

together, which is indicated by the skyrmions interacting with each other in the real-space spin figure. At a temperature higher than 6 K, the peaks join into a circle, indicating the total loss of six-fold symmetry while a dominant spin-correlation length still exists.

4.2.2 Skyrmion deformation and interaction

Here we consider the dynamics of the skyrmion structure at non-zero temperature including shape deformation and interaction of the skyrmions in different temperatures. To do this, the time evolution of the skyrmion structures has been monitored. Figure 4.5 shows snapshots of the skyrmion states at 1 ns and 2 ns at different temperatures in thermal equilibrium. At low temperature below 6 K in our case, the deformation of the skyrmion is the dominant effect of the thermal field, while at a temperature higher than 6 K, the skyrmions begin to interact and thus breaking the lattice symmetry.

At 4 K, the skyrmions change shape randomly, while not interacting with neighbors. Two skyrmions are chosen for example, which are enclosed in the solid rectangles. The sizes of these skyrmions are different, indicating different type of deformation. Skyrmion on the top shrinks with time, and skyrmion on the bottom remains the same size.

At 6 K, the skyrmions begin to interact with each other, as is shown in the top rectangle, while in the bottom rectangle there still exists individual skyrmion in thermal equilibrium. The disappearance of the skyrmion state occurs when the skyrmions begin to interact.

At 8 K, almost all the skyrmions are deformed and interacting with each other at same time, forming some random spin structure, as is shown in the chosen rectangular area. The skyrmion lattice at this temperature transits into a spin-disordered state.

4.3. PARAMETERS FOR THE PHASE DIAGRAM

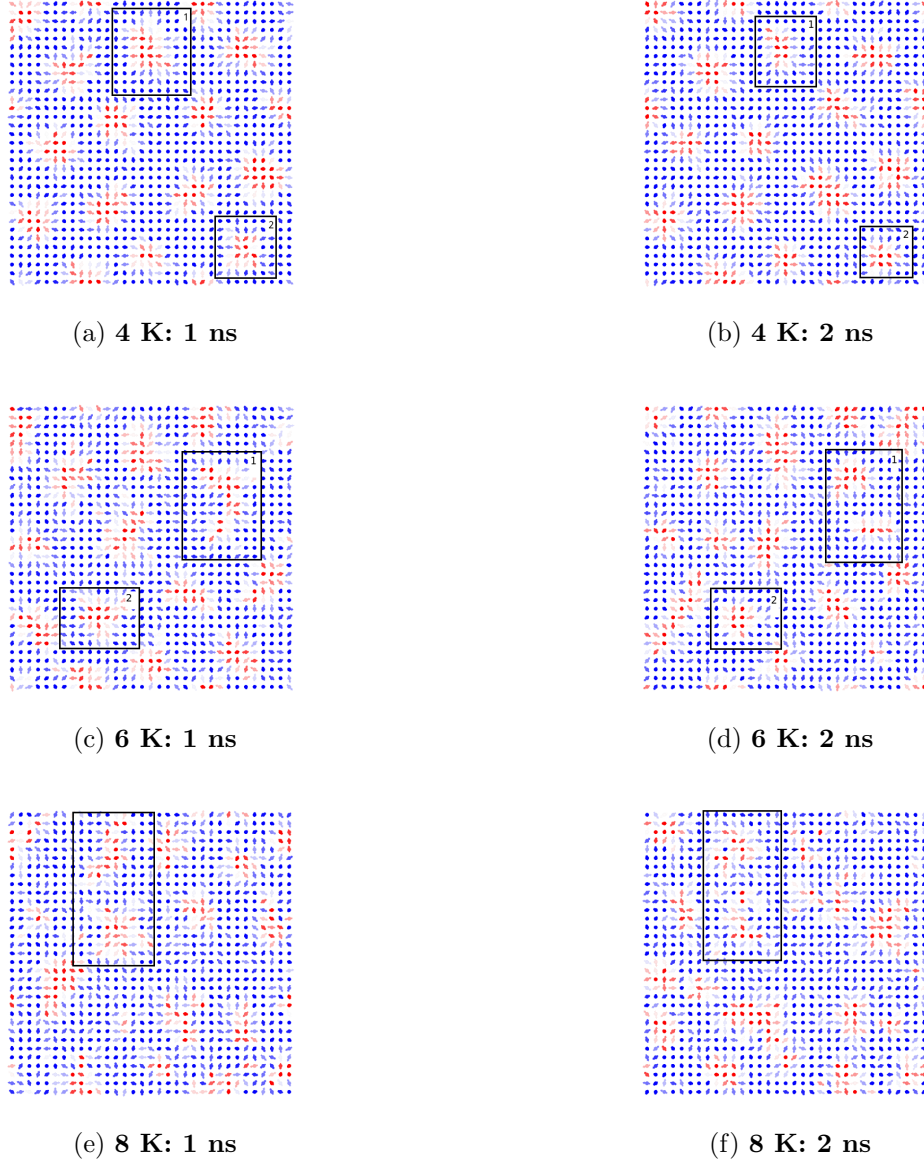


Figure 4.5: At 4 K, 6 K and 8K, two spin figures are chosen, with 1 ns time interval.

4.3 Parameters for the phase diagram

Normal parameters such as total energy E , magnetization M and the skyrmion number N change continuously with increasing temperature, as is shown in figure 4.1. In order to find the temperature-driven phase transition, two quantities named the specific heat capacity[53] and static magnetic susceptibility[54] are calculated under thermal equilibrium at each temperature. The two parameters of all five spin states will be shown, while the skyrmion state is the

main concern here.

4.3.1 Specific heat capacity

The specific heat capacity describes the variance of energy in the thermal equilibrium, as the equation:

$$C_v = \frac{\langle E^2 \rangle - \langle E \rangle^2}{NT^2}. \quad (4.3)$$

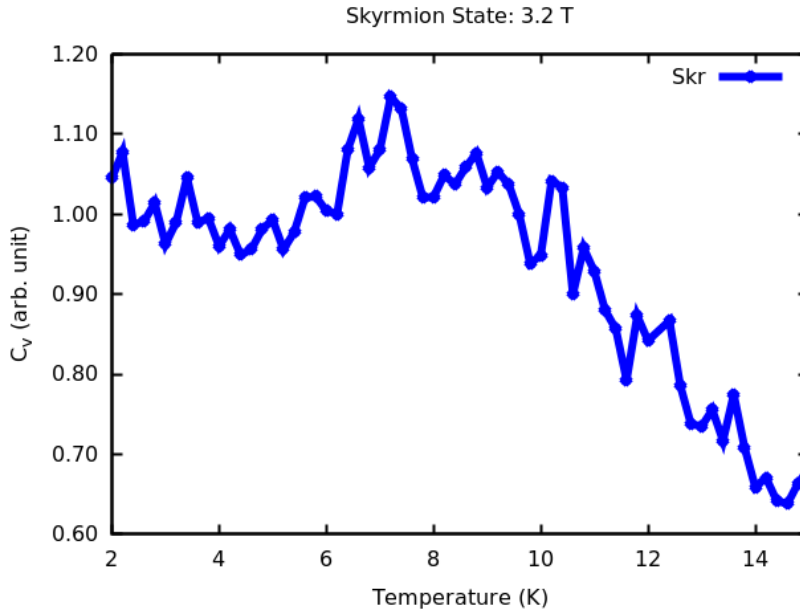


Figure 4.6: The specific heat capacity in the skyrmion state. In this state, the heat capacity shows a peak at around 6 K.

In this form, the specific heat capacity actually characterizes the thermal stability of the lattice in the skyrmion state, with varying temperature. Within $T < 6$ K region, the specific heat capacity fluctuates in a certain range. The curve features a peak at around 6 K, then decreases with increasing temperature. The breaking of the ordered skyrmion structure leads to the peak of the specific heat capacity, at a critical temperature of around 6 K.

4.3.2 Static Magnetic Susceptibility

The static magnetic susceptibility is another feature commonly used in experiments[54][55], indicating the phase transition of the spin states in the thermal field. The

4.4. SKYRMION LIFE TIME

magnetization M in equation (4.4) is an average over the whole lattice, and its statistical average is calculated in thermal equilibrium.

$$\chi = \frac{\langle M^2 \rangle - \langle M \rangle^2}{NT}. \quad (4.4)$$

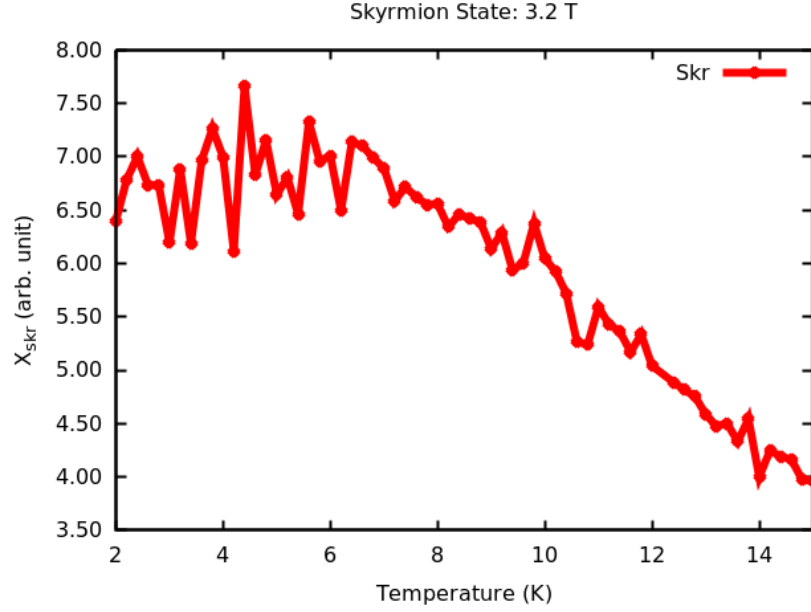


Figure 4.7: The static magnetic susceptibility in the skyrmion state. In this state, the susceptibility shows a phase change at around 6 K.

The static magnetic susceptibility clearly shows a phase change of the skyrmion state at around 6 K, with the value fluctuating from 0-6 K. The fluctuation ends at around 6 K, which is consistent with the peak point in the specific heat capacity, then decreases smoothly with increasing temperature.

4.4 Skyrmion life time

The life time of the skyrmion at a finite temperature is an important index in the theoretical study of its stability. The skyrmion life time t_{skr} is defined as the time period of one skyrmion annihilating in the lattice, thus reducing N_{skr} from 1 to 0. The procedure of calculating t_{skr} initiates with field cooling to form skyrmion lattice in 0 K in the critical perpendicular magnetic field 3.2 T, followed by an instant applied temperature after which the time dependence of

the skyrmion number is calculated.. An example of 6 K thermal field is shown in figure 4.8.

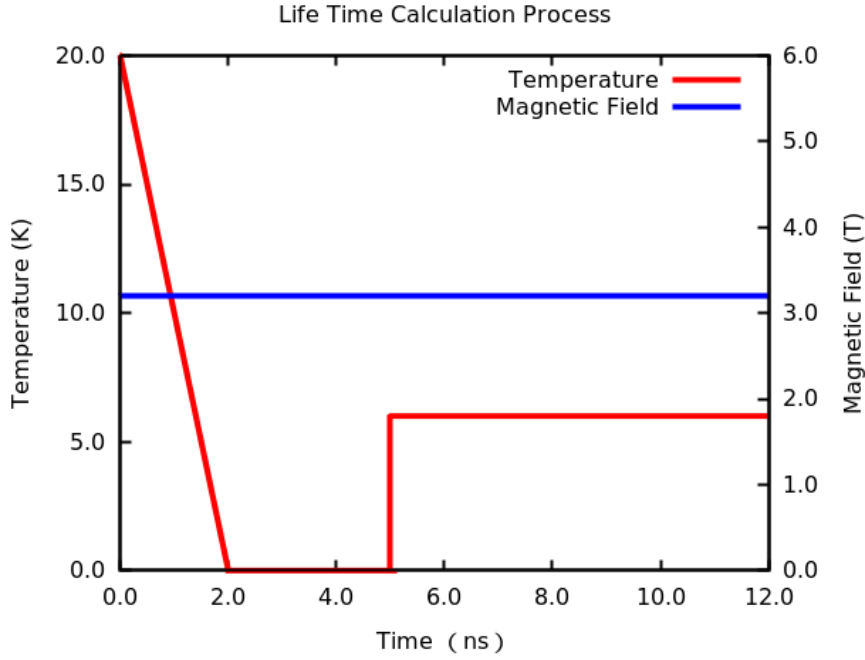


Figure 4.8: The process starts with the field cooling by 2 ns, followed by 3 ns equilibrium time in 0 K. A constant temperature of 6 K is applied at 5 ns. A constant perpendicular magnetic field of 3.2 T exists in the whole procedure.

4.4.1 Simple model of the skyrmion time decay

Several assumptions should be mentioned in the calculation of skyrmion life time due to its definition.

1. The skyrmion is supposed not to be reversed by temperature, so that the skyrmion number of a single skyrmion $N_{skr} \neq -1$ at any temperature. Specifically, the thermal field results in the skyrmion deformation and destruction, reducing N_{skr} to zero if temperature is high enough. This is tenable because the skyrmion lattice is nucleated within the stripes opposite to the perpendicular magnetic field, hence the orientation of the skyrmion depends on the direction of applied field in the case of this thesis. This assumption ensures the validity of counting the skyrmion number in revealing the skyrmion annihilation at certain temperature.

4.4. SKYRMION LIFE TIME

2. The annihilation is supposed to coexist with the creation of the skyrmion, which means the annihilation of the skyrmion is a dynamic procedure and will eventually reach a certain equilibrium skyrmion number. In other words, there is a balance between the annihilation and the creation of the skyrmion lattice. As the lattice always tends to minimize the energy, and the skyrmion state is the ground state in case of the calculation of the life time, the skyrmions are supposed to be nucleated while the existing hexagonal skyrmion lattice is being destroyed by the thermal field.
3. The skyrmion number in the life time is calculated among the skyrmion lattice as an average, instead of tracking the single skyrmion. It is hard to follow the skyrmion one by one because there is a randomness of the skyrmions behavior in the thermal field (figure 4.5).
4. In equation (4.6) no account is taken of shape changes in the skyrmions. This seems reasonable since the topological stability of the Skyrmions means that N_{skr} will not depend strongly on the skyrmion shape. This is evident in figure 3.6 where the skyrmion lattices with and without magnetic field have similar N_{skr} . However, this assumption breaks down at low temperature where the deformation of the skyrmions is the main consequence of the thermal field.

4.4.2 Calculation of the life time

Under the above-mentioned prerequisites, the time evolution of the skyrmion in a certain temperature is defined as:

$$\frac{dN_{skr}}{dt} = \frac{1}{t_{cr}} - N_{skr} \frac{1}{t_{skr}}. \quad (4.5)$$

where t_{skyr} is the skyrmion life time, t_{cr} is the creation time so that $\frac{1}{t_{cr}}$ is the creation rate of the skyrmion and $\frac{1}{t_{skyr}}$ is the annihilation rate. The underlying meaning of the equation is fairly clear: the rate of change of the skyrmion number $\frac{dN_{skr}}{dt}$ equals to the creation rate $\frac{1}{t_{cr}}$ minus the rate of decrease of the existing net skyrmions $N_{skr} \frac{1}{t_{skr}}$.

In order to fit the real data from the simulation, the N_{skr} in the equation is

4.4. SKYRMION LIFE TIME

represented as a function of real time t :

$$N_{skr} = c \cdot e^{-\frac{t}{t_{skr}}} + \frac{t_{skr}}{t_{cr}}. \quad (4.6)$$

c is an integration constant, which equals to $N_{skr} - \frac{t_{skr}}{t_{cr}}$ when $t = 0$.

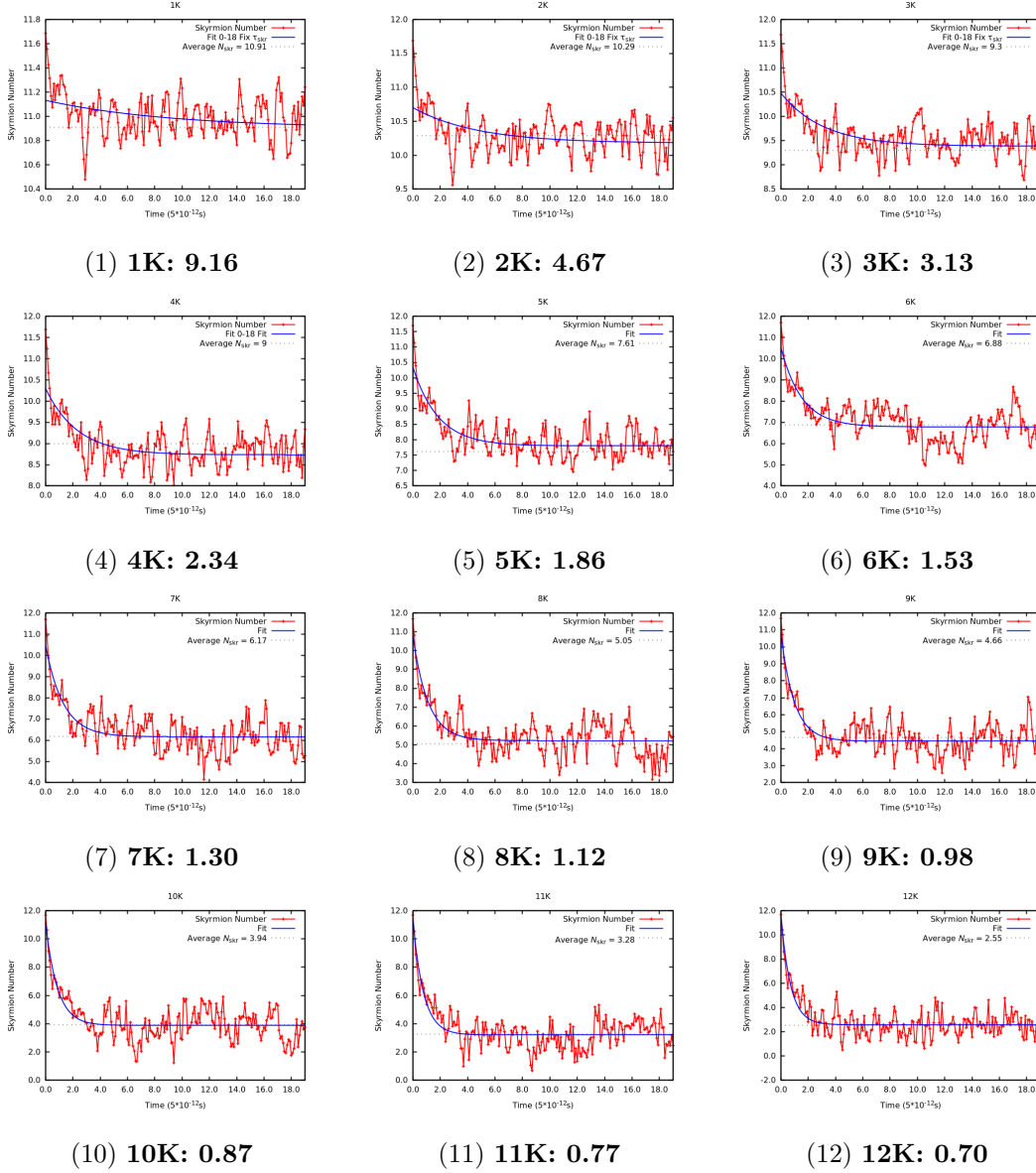


Figure 4.9: (1)-(12): the fitting of real-time data of the skyrmion number with time to (4.6) at different temperatures from 1 K to 12 K. the red line is the real skyrmion number calculated from the lattice at each time step of 5 ps, and the blue line is the fitting curve by (4.6). The number indicated showing the fitting life time of the skyrmions at each temperature in the unit of 5×10^{-12} s.

In order to fit the real-time simulations with equation (4.6), the data gath-

4.4. SKYRMION LIFE TIME

ering begins at the imposition of the step change of temperature, and lasts for 100 ps with 5 ps time step, which are long enough to cover the decay process to equilibrium at a given temperature. As shown in the contour plot and the parameters in Fig. 4.6 and Fig. 4.7, for the thermal phase transition the critical temperature is identified around 6 K, so the life time is calculated from 1 K to 12 K. From figure 4.9, the simulation data fits well with equation (4.6), as the real-time average skyrmion numbers are comparable with the theoretical skyrmion numbers under thermal equilibrium states. This further validates the assumption **2** that the skyrmions are of coexisting creation/annihilation processes of the skyrmions, yielding finite skyrmion numbers in thermal equilibrium theoretically. Note that in first few picosecond at low temperature (≤ 5), the fitting does not work well. This is due to assumption **2** that the deformation of the skyrmions is precluded in equation (4.5), which is the leading consequence of applying a step of temperature impulse at low temperature.

4.4.3 The Arrhenius Law

The skyrmion number on lattice shows the exponential decay in thermal field, yielding different skyrmion life time t_{skr} at each temperature. When the skyrmion structure undergoes a phase transition at a temperature higher than the critical point, the skyrmion life time follows an exponential rule at high temperature, which is called Arrhenius law:

$$t_{skr} = t_0 e^{\frac{\Delta E}{k_B T}}. \quad (4.7)$$

The equation (4.7) of the Arrhenius law describes the relationship between life time of the system and temperature. Note that for two temperature regions divided by the critical temperature, this empirical law is fitted with different ΔE . Since the system at a temperature lower than 6 K mainly undergoes a shape changing of the skyrmions instead of a phase transition, as is shown in section 4.2, the ΔE in this temperature region reflects the energy barrier, showing a different fitting slope from a higher temperature where the energy barrier is surmounted, thus turning into the diffusive spin state. In this case, the deviation point of the skyrmion life time at certain temperature from this

equation can be applied to denote the critical temperature of the phase transition (figure 4.10). In order to illustrate this relationship better by calculation results, the skyrmion life time is converted into logarithm scale:

$$\ln t_{skr} = t'_0 \frac{\Delta E}{k_B T}. \quad (4.8)$$

In (4.8), the logarithm skyrmion life time has a linear relationship with $\frac{1}{T}$.

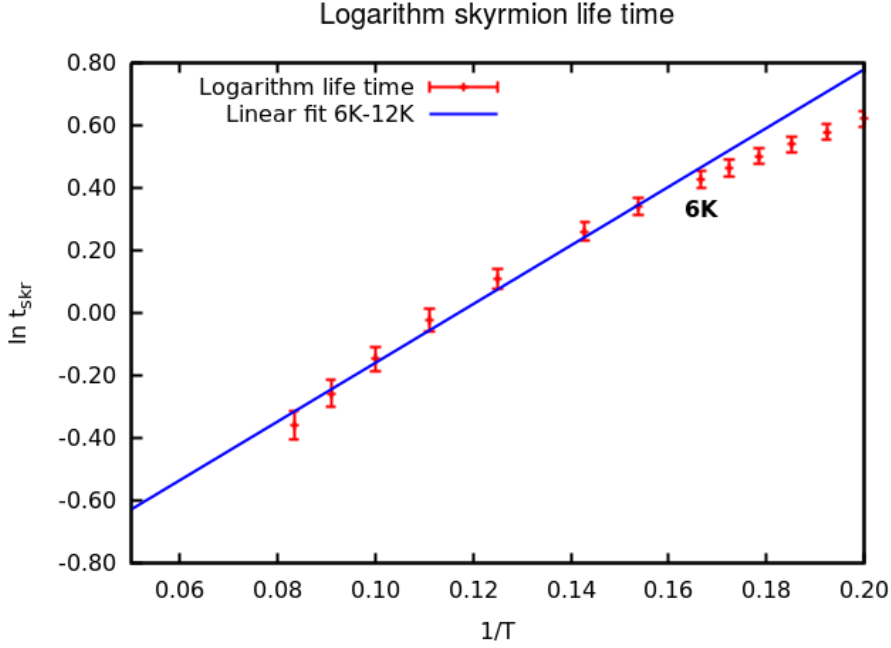


Figure 4.10: The logarithm skyrmion life time in each temperature with the error bar from the fitting in figure 4.9. The temperatures from left to right decrease from 12 K to 5 K, thus the reciprocal $1/T$ increases. The logarithm life time is fitted linearly from 12 K to 6 K, while gradually deviates from the fitting curve from 6 K to 5 K, indicating a transition from purely diffusive behavior to a topologically protected state.

The skyrmion lattice, as is mentioned, are expected to behave differently in two regions of temperature due to the topological protection. The critical temperature can thus be found by fitting the life time to equation (4.8). In the region of 12 K down to 6 K, the life time data fit linearly in the equation (4.8) where the skyrmion topological structure is destroyed, while from 6 K the logarithm skyrmion life time digressed from the fitting line, indicating a different energy barrier from higher temperature in the Arrhenius Law.

4.5 Creation of the skyrmion state by femtosecond pulse

So far in this thesis, the skyrmion state are nucleated by cooling down the lattice in certain magnetic field, while evidence shows that the shift from the spiral ground state to the skyrmion state can be achieved by ultrafast laser pulse[56]. The effect of the picosecond pulse on the skyrmion lattice are investigated computationally by the previous researches[57], while the femtosecond properties are yet to be studied. The main concern of this section is to give a preliminary study illustrating the effects of the femtosecond pulse. The femtosecond pulse has two effects. The first is a rapid increase in the conduction electron temperature which can give rise to demagnetization and the second is the possible presence of a large magnetic field associated with the inverse Faraday effect[58].The temperature pulse is applied first, followed by adding a simultaneous magnetic pulse.

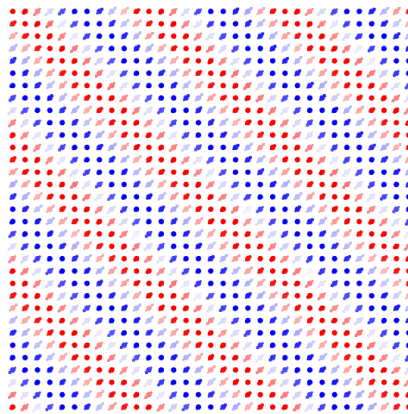


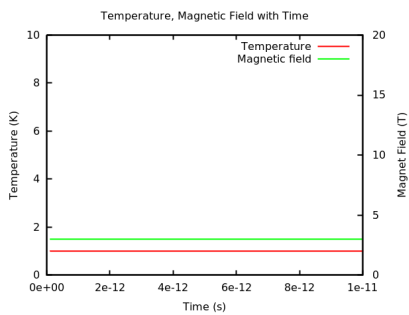
Figure 4.11: The origin spiral state for the simulations in this section.

4.5.1 Effect of femtosecond heat pulse

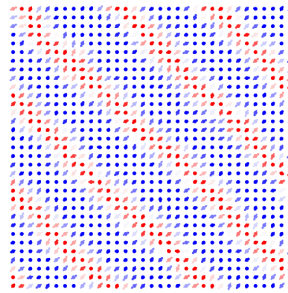
The effect of femtosecond heat pulse is studied first, since the thermal effect is the major consequence of the laser pulse. The heat pulse is expected to turn the spiral state to the skyrmion state under certain external conditions, as the previous experimental study shows. Similar to the experimental study,

4.5. CREATION OF THE SKYRMION STATE BY FEMTOSECOND PULSE

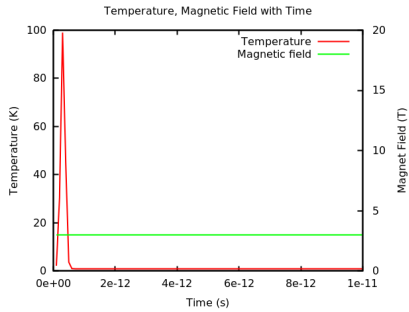
the heat pulse is set to be 100 fs. The simulations start with the spiral state (figure 4.11), with a given constant temperature and a constant magnetic field. The background temperature is set to be 1 K, which triggers the phase transition together with the pulse; a 3 T magnetic field is maintained so that the skyrmions could survive if nucleated. Three conditions are compared here: constant 1 K, 100 K heat pulse and 300 K heat pulse, as is shown in figure 4.12.



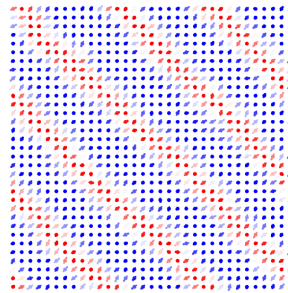
(a) **Constant 1 K**



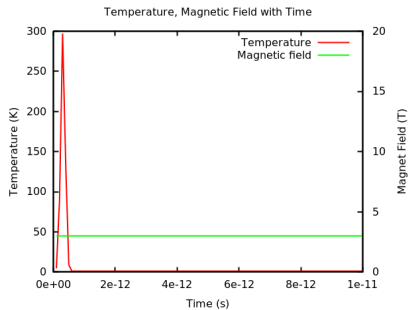
(b) **Constant 1 K**



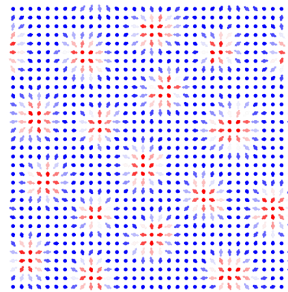
(c) **100 K Pulse**



(d) **100 K Pulse**



(e) **300 K Pulse**



(f) **300 K Pulse**

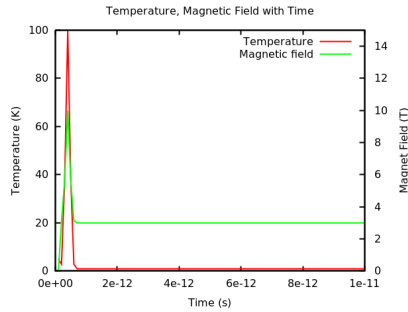
Figure 4.12: The conditions and the consequent spin figures for the heat pulse: the left column is the conditions of each simulation, and the right column shows the spin figures under each condition.

4.5. CREATION OF THE SKYRMION STATE BY FEMTOSECOND PULSE

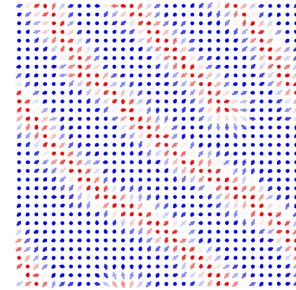
It is obvious that a sufficient intensity of the ultrafast thermal pulse leads to a phase transition from the spiral state to the skyrmion state, while a minimum thermal energy is required, 300 K in this case.

4.5.2 Additional magnetic pulse

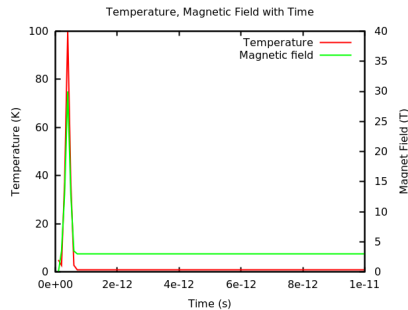
The femtosecond thermal pulse is proved to be effective in promoting the phase transition in a constant field, while in reality there could be an equivalent magnetic field coexisting with the heat pulse during a femtosecond laser pulse, due to the inverse Faraday effect. Although this type of magnetic field is largely invoked by the experimental study, its origin and magnitude remains controversial in theory. In this part, the magnetic field is set to be a simultaneous magnetic pulse with the heat pulse, and its effect is judged by the after-pulse spin figure in 10 T and 30 T with a heat pulse of 100 K.



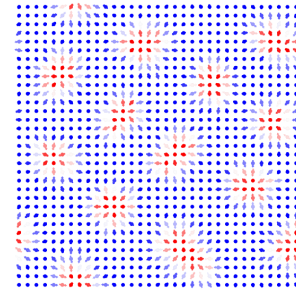
(a) 10 T Pulse



(b) 10T Pulse



(c) 30 T Pulse



(d) 30 T Pulse

Figure 4.13: The conditions and the consequent spin figures for the heat pulse and the magnetic pulse: the left column is the conditions of each simulation, and the right column shows the spin figures under each condition.

From figure 4.13, the 10 T magnetic pulse change the spin configurations, but is not strong enough for a transition to the skyrmion state. The 30 T magnetic pulse, on the other hand, gives rise to the phase transition, which is the same as a 300 K heat pulse without magnetic field. In another words, the existence of the equivalent magnetic field could help to decrease the required intensity of the heat pulse, or the intensity of the laser in the real experiment.

4.6 Summary

In this chapter, we discuss in detail the behavior of the skyrmion lattice at finite temperature, and utilize varied tools to define the thermal phase diagram of the lattice in the skyrmion state. We find the phase transition temperature is at 6 K by analyzing several parameters such as specific heat capacity, static susceptibility and the life time, together with spin configurations indicating the melting of the lattice symmetry. The effect of the femtosecond pulse on the skyrmion lattice is discussed, showing that the heat pulse is able to nucleate the skyrmion state from the ground spiral state, and an additional magnetic pulse could lower the intensity of the heat pulse for the skyrmion nucleation.

Chapter 5

Conclusion

In this thesis we conduct detailed investigations on the phase diagram of the skyrmion lattice with the DM interaction using the atomistic simulations. We develop a model of the skyrmion lattice first. For computational efficiency, the material parameters are set to be $J = D = 1$ meV, which yielding relatively small skyrmions and low critical temperature. At 0 K with the perpendicular magnetic field, the magnetic field is varied, and five spin states are thus created, including the skyrmion state. The skyrmion state is shown to exist even without the magnetic field. The ratio between the exchange interaction and the DM interaction influences the size of the skyrmion, and the in-plane and out-of-plane anisotropy is another factor affecting the size and shape of skyrmions.

Then, the skyrmion lattice is exposed to the thermal field in order to develop a complete phase diagram of the skyrmion state. An equilibrium contour plot of the skyrmion number of the skyrmion state over temperature and magnetic field is shown. An estimated critical temperature from the topological energy barrier is around 6 K, which corresponds to 0.51 meV in the unit of D^2/J . The spin figures in real and momentum space are studied, showing a melting of the lattice symmetry at 6 K. Further parameters, including the specific heat capacity and the static magnetic susceptibility reveal a phase transition occurs at 6 K. The skyrmion life time indicates the phase transition of the skyrmion state at 6 K and higher follows the Arrhenius law. Finally, a preliminary study of the femtosecond pulse on the skyrmion lattice shows that the heat

and magnetic pulse can be implemented as one alternative way to nucleate the skyrmion state.

The methodology in this thesis is of broad applicability and can be applied to other computational studies of the skyrmion phase diagram. we focus on a bottom-up development of the phase diagram, from the ground state in 0 K to the thermal stability of the skyrmion state. As discussed in chapter 4, the phase transition of the skyrmion state can be judged from the spin configurations of the lattice at different temperature, indicating a destruction of the six-fold symmetry by the skyrmion interaction above the critical temperature. The transition point can be further examined and quantified by introducing the specific heat capacity, the static magnetic susceptibility and the skyrmion life time mentioned in this thesis. While the material parameters of the skyrmion lattice is not realistic in this thesis, the underlying physics is expected to be the same with the simulations of real materials.

5.0.1 Future outlook

The present work can be continued by developing the phase diagram of the real-world skyrmion systems. In this case, the simulation scale will be expanded to several hundreds of nanometers due to a small ratio of DM interaction and exchange interaction in real materials, yielding much larger skyrmions comparing with the present thesis. The simulation may also be extended to including several layers of materials with strong spin-orbit interaction, which is the case of the current room-temperature skyrmions.

Another extension of this work is to include the spin transfer torque into the nucleation and the dynamics of the skyrmion system. Specifically, the skyrmion dynamics by spin-current is intensively studied so far, while the thermal effect on the moving skyrmions is yet to be investigated. The challenging task will be the simulation of the combination of the nucleation, phase diagram and dynamics of the skyrmion at room temperature.

Last but not the least, the ultrafast optical control of the skyrmion lattice can be further investigated. As the laser is simply considered as the heat and magnetic pulse in this thesis, several detailed properties such as the two-

temperature model and the effect of polarized light can be take into account. To sum up, the research on skyrmions is one of the most attracting topics in spintronics, and the findings in our thesis contributes to the computational study on skyrmions.

Appendix A

The skyrmion number on a discrete lattice

In this thesis we have used a discrete approximation to calculation the skyrmion number, based on the continuum expression in equation (A.1).

$$N_{skr} = \frac{1}{4\pi} \iint dx dy \mathbf{n} \cdot \left(\frac{\partial \mathbf{n}}{\partial x} \times \frac{\partial \mathbf{n}}{\partial y} \right). \quad (\text{A.1})$$

The first step is to make a clear definition of the variables. x and y are discrete positive integers denoting the space coordinate of the two-dimension lattice, while \mathbf{n} is the three dimension spin vector denoted as \mathbf{n}_i , \mathbf{n}_j and \mathbf{n}_k . In this case, one spin on the lattice is characterized by the spin direction and its position on the lattice. For example, the i component of a spin in the lattice position $x = 1$ and $y = 2$ can be expressed as $\mathbf{n}_i^{1,2}$. The constant $\frac{1}{4\pi}$ is a normalization factor, which ensures a single skyrmion structure yielding $N_{skr} = 1$.

The second step is to calculate the cross product of the partial derivatives in equation (A.1). Since the skyrmion lattice in the thesis is set to be discrete, the partial derivative of the spin vector \mathbf{n} over the lattice coordinate x and y can be written as:

$$\begin{aligned} \frac{\partial \mathbf{n}}{\partial x} &= \mathbf{n}^{x+1,y} - \mathbf{n}^{x,y}, \\ \frac{\partial \mathbf{n}}{\partial y} &= \mathbf{n}^{x,y+1} - \mathbf{n}^{x,y}. \end{aligned} \quad (\text{A.2})$$

Based on equation (A.2), the cross product of the partial derivatives is then calculated, and written separately in three dimensions of the spin vector:

$$\begin{aligned}
\left(\frac{\partial \mathbf{n}}{\partial x} \times \frac{\partial \mathbf{n}}{\partial y}\right)_i &= (\mathbf{n}_j^{x+1,y} - \mathbf{n}_j^{x,y}) \cdot (\mathbf{n}_k^{x,y+1} - \mathbf{n}_k^{x,y}) - (\mathbf{n}_k^{x+1,y} - \mathbf{n}_k^{x,y}) \cdot (\mathbf{n}_j^{x,y+1} - \mathbf{n}_j^{x,y}); \\
\left(\frac{\partial \mathbf{n}}{\partial x} \times \frac{\partial \mathbf{n}}{\partial y}\right)_j &= (\mathbf{n}_k^{x+1,y} - \mathbf{n}_k^{x,y}) \cdot (\mathbf{n}_i^{x,y+1} - \mathbf{n}_i^{x,y}) - (\mathbf{n}_i^{x+1,y} - \mathbf{n}_i^{x,y}) \cdot (\mathbf{n}_k^{x,y+1} - \mathbf{n}_k^{x,y}); \\
\left(\frac{\partial \mathbf{n}}{\partial x} \times \frac{\partial \mathbf{n}}{\partial y}\right)_k &= (\mathbf{n}_i^{x+1,y} - \mathbf{n}_i^{x,y}) \cdot (\mathbf{n}_j^{x,y+1} - \mathbf{n}_j^{x,y}) - (\mathbf{n}_j^{x+1,y} - \mathbf{n}_j^{x,y}) \cdot (\mathbf{n}_i^{x,y+1} - \mathbf{n}_i^{x,y}).
\end{aligned} \tag{A.3}$$

The final step is to calculate the skyrmion number in the discrete lattice model. The discretization of equation (A.1) includes an alter from integral formula to a sum formula. Thus N_{skr} can be calculated as a sum over three dimensions of the spin vector:

$$N_{skr,i} = N_{skr,i} + N_{skr,j} + N_{skr,k}, \tag{A.4}$$

In each dimension, the component of the N_{skr} can be expressed as a sum over the whole lattice (suppose the lattice consists of $m \times m$ lattice points):

$$\begin{aligned}
N_{skr,i} &= \frac{1}{4\pi} \sum_x^{m-1} \sum_y^{m-1} \mathbf{n}_i^{x,y} \cdot [(\mathbf{n}_j^{x+1,y} - \mathbf{n}_j^{x,y}) \cdot (\mathbf{n}_k^{x,y+1} - \mathbf{n}_k^{x,y}) - \\
&\quad (\mathbf{n}_k^{x+1,y} - \mathbf{n}_k^{x,y}) \cdot (\mathbf{n}_j^{x,y+1} - \mathbf{n}_j^{x,y})] \\
N_{skr,j} &= \frac{1}{4\pi} \sum_x^{m-1} \sum_y^{m-1} \mathbf{n}_j^{x,y} \cdot [(\mathbf{n}_k^{x+1,y} - \mathbf{n}_k^{x,y}) \cdot (\mathbf{n}_i^{x,y+1} - \mathbf{n}_i^{x,y}) - \\
&\quad (\mathbf{n}_i^{x+1,y} - \mathbf{n}_i^{x,y}) \cdot (\mathbf{n}_k^{x,y+1} - \mathbf{n}_k^{x,y})] \\
N_{skr,k} &= \frac{1}{4\pi} \sum_x^{m-1} \sum_y^{m-1} \mathbf{n}_k^{x,y} \cdot [(\mathbf{n}_i^{x+1,y} - \mathbf{n}_i^{x,y}) \cdot (\mathbf{n}_j^{x,y+1} - \mathbf{n}_j^{x,y}) - \\
&\quad (\mathbf{n}_j^{x+1,y} - \mathbf{n}_j^{x,y}) \cdot (\mathbf{n}_i^{x,y+1} - \mathbf{n}_i^{x,y})].
\end{aligned} \tag{A.5}$$

The equation (A.4) and (A.5) are discrete expression of calculating N_{skr} .

Bibliography

- [1] I Kézsmárki, S Bordács, P Milde, E Neuber, LM Eng, JS White, Henrik M Rønnow, CD Dewhurst, M Mochizuki, K Yanai, et al. Néel-type skyrmion lattice with confined orientation in the polar magnetic semiconductor *gav4s8*. *Nature materials*, 14(11):1116–1122, 2015.
- [2] Hannay J D. *Computational simulations of thermally activated magnetization dynamics at high frequencies*. PhD thesis, School of Informatics, University of Wales, 2001.
- [3] T. H. R. Skyrme. A unified theory of mesons and baryons. *Nuclear Physics*, 10, 1962.
- [4] A. O. Leonov, I. E. Dragunov, U. K. Röbner, and A. N. Bogdanov. Theory of skyrmion states in liquid crystals. *Phys. Rev. E*, 90:042502, Oct 2014.
- [5] Richard A Battye, NR Cooper, and Paul M Sutcliffe. Stable skyrmions in two-component bose-einstein condensates. *Physical review letters*, 88(8):080401, 2002.
- [6] UK Röbner, AN Bogdanov, and C Pfeleiderer. Spontaneous skyrmion ground states in magnetic metals. *Nature*, 442(7104):797–801, 2006.
- [7] AN Bogdanov and DA Yablonskii. Thermodynamically stable” vortices” in magnetically ordered crystals. the mixed state of magnets. *Zh. Eksp. Teor. Fiz*, 95:182, 1989.
- [8] A Bogdanov and A Hubert. Thermodynamically stable magnetic vortex states in magnetic crystals. *Journal of magnetism and magnetic materials*, 138(3):255–269, 1994.

BIBLIOGRAPHY

- [9] UK Rößler, AN Bogdanov, and C Pfleiderer. Spontaneous skyrmion ground states in magnetic metals. *Nature*, 442(7104):797–801, 2006.
- [10] S Mühlbauer, B Binz, F Jonietz, C Pfleiderer, A Rosch, A Neubauer, R Georgii, and P Böni. Skyrmion lattice in a chiral magnet. *Science*, 323(5916):915–919, 2009.
- [11] A Neubauer, C Pfleiderer, B Binz, A Rosch, R Ritz, PG Niklowitz, and P Böni. Topological hall effect in the a phase of mnsi. *Physical review letters*, 102(18):186602, 2009.
- [12] C Pappas, E Lelievre-Berna, P Falus, PM Bentley, E Moskvina, S Grigoriev, P Fouquet, and B Farago. Chiral paramagnetic skyrmion-like phase in mnsi. *Physical review letters*, 102(19):197202, 2009.
- [13] Stefan Heinze, Kirsten Von Bergmann, Matthias Menzel, Jens Brede, André Kubetzka, Roland Wiesendanger, Gustav Bihlmayer, and Stefan Blügel. Spontaneous atomic-scale magnetic skyrmion lattice in two dimensions. *Nature Physics*, 7(9):713–718, 2011.
- [14] Naoto Nagaosa and Yoshinori Tokura. Topological properties and dynamics of magnetic skyrmions. *Nature nanotechnology*, 8(12):899–911, 2013.
- [15] Ganna Butenko. Phenomenological theory of chiral states in magnets with dzyaloshinskii-moriya interactions. 2012.
- [16] AR Fert. Magnetic and transport properties of metallic multilayers. In *Materials Science Forum*, volume 59, pages 439–480. Trans Tech Publ, 1990.
- [17] Gong Chen, Arantzazu Mascarague, Andreas K Schmid, et al. Room temperature skyrmion ground state stabilized through interlayer exchange coupling. *Applied Physics Letters*, 106(24):242404, 2015.
- [18] R Tomasello, E Martinez, R Zivieri, L Torres, M Carpentieri, and G Finocchio. A strategy for the design of skyrmion racetrack memories. *arXiv preprint arXiv:1409.6491*, 2014.

- [19] NS Kiselev, AN Bogdanov, R Schäfer, and UK Rößler. Chiral skyrmions in thin magnetic films: new objects for magnetic storage technologies? *Journal of Physics D: Applied Physics*, 44(39):392001, 2011.
- [20] Albert Fert, Vincent Cros, and João Sampaio. Skyrmions on the track. *Nature nanotechnology*, 8(3):152–156, 2013.
- [21] Dhritiman Bhattacharya, Md Mamun Al-Rashid, and Jayasimha Atulasimha. Voltage controlled core reversal of fixed magnetic skyrmions without a magnetic field. *arXiv preprint arXiv:1603.00927*, 2016.
- [22] R F L Evans, W J Fan, P Chureemart, T A Ostler, M O A Ellis, and R W Chantrell. Atomistic spin model simulations of magnetic nanomaterials. *Journal of Physics: Condensed Matter*, 26, 2014.
- [23] Mohsen Razavy. *Heisenberg’s quantum mechanics*. World Scientific, 2011.
- [24] David Jiles. *Introduction to Magnetism and Magnetic Materials*. CRC Press, third edition edition, 2016.
- [25] T L Mitran, Adela Nicolaev, G A Nemnes, L Ion, and S Antohe. Magnetic behavior and clustering effects in mn-doped boron nitride sheets. *Journal of Physics: Condensed Matter*, 24(32):326003, 2012.
- [26] James P. Sethna, Karin Dahmen, Sivan Kartha, James A. Krumhansl, Bruce W. Roberts, and Joel D. Shore. Hysteresis and hierarchies: Dynamics of disorder-driven first-order phase transformations. *Phys. Rev. Lett.*, 70:3347–3350, May 1993.
- [27] Ralph Skomski. *Simple Models of Magnetism*. Oxford University Press, 2012.
- [28] I. Dzyaloshinsky. A thermodynamic theory of “weak” ferromagnetism of antiferromagnetics. *Journal of Physics and Chemistry of Solids*, 4(4):241–255, 1958.
- [29] Tôru Moriya. Anisotropic superexchange interaction and weak ferromagnetism. *Phys. Rev.*, 120:91–98, Oct 1960.

BIBLIOGRAPHY

- [30] Matthias Bode, M Heide, K Von Bergmann, P Ferriani, S Heinze, G Bihlmayer, A Kubetzka, O Pietzsch, S Blügel, and R Wiesendanger. Chiral magnetic order at surfaces driven by inversion asymmetry. *Nature*, 447(7141):190–193, 2007.
- [31] G. Chen, J. Zhu, A. Quesada, J. Li, A. T. N’Diaye, Y. Huo, T. P. Ma, Y. Chen, H. Y. Kwon, C. Won, Z. Q. Qiu, A. K. Schmid, and Y. Z. Wu. Novel chiral magnetic domain wall structure in Fe/Ni/Cu(001) films. *Phys. Rev. Lett.*, 110:177204, Apr 2013.
- [32] A. Hrabec, N. A. Porter, A. Wells, M. J. Benitez, G. Burnell, S. McVitie, D. McGrouther, T. A. Moore, and C. H. Marrows. Measuring and tailoring the dzyaloshinskii-moriya interaction in perpendicularly magnetized thin films. *Phys. Rev. B*, 90:020402, Jul 2014.
- [33] E. Simon, K. Palotás, L. Rózsa, L. Udvardi, and L. Szunyogh. Formation of magnetic skyrmions with tunable properties in pdfe bilayer deposited on ir(111). *Phys. Rev. B*, 90:094410, Sep 2014.
- [34] Kamel Ounadjela Burkard Hillebrands. *Spin Dynamics in Confined Magnetic Structures*. Springer, 2001.
- [35] TL Gilbert. A lagrangian formulation of the gyromagnetic equation of the magnetization field. *Phys. Rev.*, 100:1243, 1955.
- [36] M Lakshmanan. The fascinating world of the landau–lifshitz–gilbert equation: an overview. *Philosophical Transactions of the Royal Society of London A: Mathematical, Physical and Engineering Sciences*, 369(1939):1280–1300, 2011.
- [37] Ryoichi Kikuchi. On the minimum of magnetization reversal time. *Journal of Applied Physics*, 27(11):1352–1357, 1956.
- [38] William Fuller Brown Jr. Thermal fluctuation of fine ferromagnetic particles. *Magnetics, IEEE Transactions on*, 15(5):1196–1208, 1979.

- [39] García-Palacios, José Luis, Lázaro, and Francisco J. Langevin-dynamics study of the dynamical properties of small magnetic particles. *Phys. Rev. B*, 58:14937–14958, Dec 1998.
- [40] Nicholas Metropolis and Stanislaw Ulam. The monte carlo method. *Journal of the American statistical association*, 44(247):335–341, 1949.
- [41] N. R. Cooper and D. B. Chklovskii. Theory of photoluminescence of the $\nu=1$ quantum hall state: Excitons, spin-waves and spin-textures. *Phys. Rev. B*, 55, 1997.
- [42] N. R. Cooper. Skyrmions in quantum hall systems with realistic force-laws. *Phys. Rev. B*, 55, 1997.
- [43] Usama Al Khawaja and Henk Stoof. Skyrmions in a ferromagnetic bose–einstein condensate. *Nature*, 411, 21 June 2001.
- [44] C. M. Savage and J. Ruostekoski. Energetically stable particlelike skyrmions in a trapped bose-einstein condensate. *Phys. Rev. Lett.*, 91, 1 July 2001.
- [45] A. O. Leonov, I. E. Dragunov, U. K. Röbner, and A. N. Bogdanov. Theory of skyrmion states in liquid crystals. *Phys. Rev. E*, 90, 15 October 2014.
- [46] Motohiko Ezawa. Giant skyrmions stabilized by dipole-dipole interactions in thin ferromagnetic films. *Phys. Rev. Lett.*, 105:197202, Nov 2010.
- [47] Tsuyoshi Okubo, Sungki Chung, and Hikaru Kawamura. Multiple- q states and the skyrmion lattice of the triangular-lattice heisenberg antiferromagnet under magnetic fields. *Phys. Rev. Lett.*, 108:017206, Jan 2012.
- [48] Motohiko Ezawa. Compact merons and skyrmions in thin chiral magnetic films. *Phys. Rev. B*, 83:100408, Mar 2011.
- [49] Junichi Iwasaki, Masahito Mochizuki, and Naoto Nagaosa. Universal current-velocity relation of skyrmion motion in chiral magnets. *Nature communications*, 4:1463, 2013.

BIBLIOGRAPHY

- [50] Rick Keesman, AO Leonov, Stefan Buhrandt, GT Barkema, Lars Fritz, and RA Duine. Néel skyrmions in confined geometries and at nonzero temperatures. *arXiv preprint arXiv:1506.00271*, 2015.
- [51] MN Wilson, AB Butenko, AN Bogdanov, and TL Monchesky. Chiral skyrmions in cubic helimagnet films: The role of uniaxial anisotropy. *Physical Review B*, 89(9):094411, 2014.
- [52] HY Kwon, KM Bu, YZ Wu, and C Won. Effect of anisotropy and dipole interaction on long-range order magnetic structures generated by dzyaloshinskii–moriya interaction. *Journal of Magnetism and Magnetic Materials*, 324(13):2171–2176, 2012.
- [53] M C Ambrose and R L Stamps. Melting of hexagonal skyrmion states in chiral magnets. *New Journal of Physics*, 15(5):053003, 2013.
- [54] A. Bauer and C. Pfleiderer. Magnetic phase diagram of mnsi inferred from magnetization and ac susceptibility. *Phys. Rev. B*, 85:214418, Jun 2012.
- [55] M. Janoschek, M. Garst, A. Bauer, P. Krautscheid, R. Georgii, P. Böni, and C. Pfleiderer. Fluctuation-induced first-order phase transition in dzyaloshinskii-moriya helimagnets. *Phys. Rev. B*, 87:134407, Apr 2013.
- [56] N Ogawa, S Seki, and Y Tokura. Ultrafast optical excitation of magnetic skyrmions. *Scientific reports*, 5, 2015.
- [57] C Heo. Statics and dynamics of magnetic skyrmions in ultrathin nanomagnets. 2015.
- [58] CD Stanciu, F Hansteen, AV Kimel, A Kirilyuk, A Tsukamoto, A Itoh, and Th Rasing. All-optical magnetic recording with circularly polarized light. *Physical review letters*, 99(4):047601, 2007.